



UNIVERSIDADE FEDERAL DO CEARÁ  
CENTRO DE TECNOLOGIA  
DEPARTAMENTO DE ENGENHARIA QUÍMICA  
PROGRAMA DE PÓS-GRADUAÇÃO EM ENGENHARIA QUÍMICA

FEDERICO LEANDRO GRECO MELO

DIFFUSION OF N-PARAFFINS IN CARBONACEOUS MATERIALS

FORTALEZA  
2015

FEDERICO LEANDRO GRECO MELO

DIFFUSION OF N-PARAFFINS IN CARBONACEOUS MATERIALS

Dissertação de Mestrado apresentada no Programa de Pós-Graduação em Engenharia Química, da Universidade Federal do Ceará, como requisito parcial para obtenção do título de Mestre em Engenharia Química.

**Orientador:** Prof. Dr. Moisés Bastos Neto

**Coorientador:** Prof. Dr. Célio Loureiro Cavalcante Jr.

FORTALEZA  
2015

Dados Internacionais de Catalogação na Publicação  
Universidade Federal do Ceará  
Biblioteca de Pós-Graduação em Engenharia - BPGE

---

M485d      Melo, Federico Leandro Greco.  
Diffusion of n-paraffins in carbonaceous materials / Federico Leandro Greco Melo. – 2015.  
74 f. : il. color. enc. ; 30 cm.

Dissertação (mestrado) – Universidade Federal do Ceará, Centro de Tecnologia, Departamento de Engenharia Química, Programa de Pós-Graduação em Engenharia Química, Fortaleza, 2015.  
Área de Concentração: Processos Químicos e Bioquímicos.  
Orientação: Prof. Dr. Moisés Bastos Neto.  
Coorientação: Prof. Dr. Célio Loureiro Cavalcante Jr.

1. Engenharia química. 2. Carbono ativado. 3. Difusão. 4. Hidrocarbonetos. I. Título.

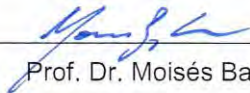
FEDERICO LEANDRO GRECO MELO

DIFFUSION OF N-PARAFFINS IN CARBONACEOUS MATERIALS

Dissertação de Mestrado apresentada ao Programa de Pós-Graduação em Engenharia Química, do Departamento de Engenharia Química, do Centro de Tecnologia, da Universidade Federal do Ceará, como requisito parcial para obtenção do Título de Mestre em Engenharia Química. Área de concentração: Adsorção.

Aprovado em: 28/09/2015

BANCA EXAMINADORA



Prof. Dr. Moisés Bastos Neto (Orientador)  
Universidade Federal do Ceará (UFC)



Prof. Dr. Sebastião Mardônio Pereira de Lucena  
Universidade Federal do Ceará (UFC)



Prof.ª Dr.ª Artemis Pessoa Guimarães  
Universidade da Integração Internacional da Lusofonia Afro-Brasileira (UNILAB)

*Aos meus pais.*

## **ACKNOWLEDGMENTS**

I am deeply grateful to my thesis advisor, Professor Moisés Bastos Neto, for his guidance, support, patience, encouragement and trust. I have benefitted from his high standard of accomplishment, his philosophy of research and his open-minded approach to new ideas.

A special thanks to Professor Célio L. Cavalcante Jr. who gave me opportunities that I have never imagined and to trust on me as a master student.

A special thanks to Professor Stefano Brandani and to Professor Enzo Mangano from the University of Edinburgh. Without their support and knowledge the research with ZLC would be tougher than it is.

Thanks to my colleagues and friends at the Universidade Federal do Ceará (UFC) and the research group. Particularly Breno Moraes, who helped me during the development of the research and the discussion about the results found.

Finally and not less important, I wish to express my deepest gratitude to my parents, Roberto Greco and Adriana Melo, to my sisters, Lorena Greco e Natacha Greco, to my girlfriend, Mariana Dobel, and to my grandparent and his wife, José Maria Melo and Jânia Melo, for their unwavering love and support, for their encouragement and motivation.

## RESUMO

A profunda compreensão dos mecanismos difusivos em sólidos porosos é essencial para o desenvolvimento de vários processos envolvendo catálise heterogênea. A impregnação de metais em suporte poroso é, geralmente, uma forma eficaz de aumentar a eficiência do catalisador. No entanto, os efeitos de tal procedimento sobre as propriedades de transporte ainda são pouco conhecidos. Zeólitas, sílicas e aluminas são os suportes mais frequentemente utilizados para catalisadores heterogêneos. Atualmente, utilizam-se também carbonos ativados (AC) como suportes, porém, apesar das várias vantagens potenciais (por exemplo, áreas de superfície bastante específicas), pouco tem sido estudado em relação ao comportamento difusivo nestes materiais. A Síntese de Fischer-Tropsch (FTS) é um processo que pode ser beneficiado com a utilização de materiais à base de carbono impregnados. Dessa forma, o método Zero Length Column (ZLC) foi aplicado neste estudo para avaliar a difusão de *n*-heptano e *n*-octano, produtos relevantes do FTS, em materiais à base de carbono antes e após a impregnação com Fe com o objetivo de investigar a cinética sob as condições normais de temperatura de FTS e determinar se os produtos do processo apresentam uma resistência significativa para o processo.

Palavras chave: difusão, ZLC, carbono ativado, FTS, parafinas lineares

## ABSTRACT

A deep understanding of the diffusion mechanisms in porous solids is essential to the development of many processes involving heterogeneous catalysis. The impregnation of metals on porous supports is generally an effective way of increasing the catalyst efficiency, but the effects of such procedure on the transport properties are poorly known. Zeolite, silica and alumina are most frequently used as supports for heterogeneous catalysts. Despite the several potential advantages of using activated carbon (AC) as supports (e.g. high specific surface areas), little has been studied regarding diffusion behavior in these materials. The Fischer-Tropsch Synthesis (FTS) is a process which could benefit from the use of carbon-based impregnated materials. The *Zero Length Column* (ZLC) method was applied in this study to evaluate the diffusion of *n*-heptane and *n*-octane, relevant products of the FTS, in carbon-based materials before and after impregnation with Fe. The aim was to investigate the kinetics under the usual temperature conditions of the FTS and determine if the products diffusion poses a significant resistance for the process.

Keywords: diffusion, paraffins, ZLC, FTS, activated carbon



## LIST OF FIGURES

Figure 1 - Main resistances to mass transfer in porous solids [24].	22
Figure 2 - Molecular diffusion mechanism [21].	23
Figure 3 - Knudsen diffusion mechanism [21].	24
Figure 4 - Schematic production of PMC1 [44].	30
Figure 5 - ZLC Scheme.	33
Figure 6 - ZLC Apparatus.	34
Figure 7 - ZLC Column.	34
Figure 8 - ZLC Column placed in the system.	35
Figure 9 - ZLC experimental signal showing the upper ( $\sigma_0$ ) and lower ( $\sigma_\infty$ ) baselines.	36
Figure 10 - Plot of normalized concentration versus time.	37
Figure 11 - Perfectly mixed cell.	39
Figure 14 - N <sub>2</sub> adsorption desorption isotherms of: (a) PMC1; (b) PMC2 [45].	45
Figure 15 - N <sub>2</sub> adsorption desorption isotherms of: (a) Fe-PMC1; (b) Fe-PMC2 [45].	46
Figure 16 - Pore size distribution of the supports: (a) PMC1; (b) PMC2. GCMC = grand canonical Monte Carlo calculations [45].	47
Figure 17 - Pore size distribution of the catalysts: (a) Fe-PMC1 and (b) Fe-PMC2. GCMC = grand canonical Monte Carlo calculations [45].	47
Figure 18 - SEM microphotographs of Fe-PMC1.	49
Figure 19 - SEM microphotographs of Fe-PMC2.	49
Figure 20 - Comparison of experimental ZLC response curves of PMC1 at P <sub>0</sub> = 0.0054 bar of <i>n</i> -C <sub>7</sub> in two different purge gas (He and N <sub>2</sub> ), 270 °C, 20 and 30 cc/min.	52
Figure 21 - Comparison of experimental ZLC response curves of Fe-PMC1 at P <sub>0</sub> = 0.0054 bar of <i>n</i> -C <sub>7</sub> in two different purge gas (He and N <sub>2</sub> ), 270 °C, 20 and 30 cc/min.	52
Figure 22 - Comparison of experimental ZLC response curves of PMC2 at P <sub>0</sub> = 0.0054 bar of <i>n</i> -C <sub>7</sub> in two different purge gas (He and N <sub>2</sub> ), 270 °C, 20 and 30 cc/min.	53

Figure 23 - Comparison of experimental ZLC response curves of Fe-PMC2 at $P_o = 0.0054$ bar of $n\text{-C}_7$ in two different purge gas (He and $\text{N}_2$ ), 270 °C, 20 and 30 cc/min. .....	53
Figure 24 - Plot for $n$ -heptane at 270 °C and $P_o = 0.0054$ bar in the Ft form (a) PMC1 (b) Fe-PMC1.....	54
Figure 25 - Plot for $n$ -heptane at 270 °C and $P_o = 0.0054$ bar in the Ft form (a) PMC2 (b) Fe-PMC2.....	54
Figure 26- Plot of desorption curves for Fe-PMC1 at 270 °C and $P_o = 0.0054$ bar of $n\text{-C}_7$ . .....	55
Figure 27 - Variation of $\beta_1$ with L according to equation 10. ....	55
Figure 28 - Influence of the saturation time in experimental ZLC desorption curves for PMC2 at $P_o = 0.0054$ bar of $n\text{-C}_7$ with He purge gas, 210 °C, 20 cc/min.....	59
Figure 29 - Influence of the saturation time in experimental ZLC desorption curves for PMC2 at $P_o = 0.0054$ bar of $n\text{-C}_8$ with He purge gas, 240 °C, 20 cc/min.....	60
Figure 30 - Influence of the flow rate on desorption plot.....	61
Figure 31 - ZLC Desorption Curves for $n\text{-C}_8$ in PMC2 showing the effects of temperature. Purge gas He at 73 cc/min. ....	62
Figure 32 - Effect of sample quantity in the macropore reciprocal diffusional time constant.....	63
Figure 33 - Effect of nonlinear equilibrium on the apparent diffusivity obtained from the application of the LT asymptote analysis. $\lambda = 0.1, 0.2, 0.3, 0.4, 0.5, 0.6, 0.7, 0.8$ [39]. ....	65
Figure 34 - Desorption response curves of $n\text{-C}_7$ in PMC2 at 270 °C and $c_o = 25$ ppm. .....	66
Figure 35 - Desorption response curves of $n\text{-C}_7$ in PMC2 at 270 °C and $c_o = 5370$ ppm. ....	66
Figure 36 - ZLC experimental signal of $n$ -dodecane at 210 °C.....	69

## LIST OF TABLES

Table 1 - Operational conditions of FTS.....	19
Table 2 - ZLC historical development.....	25
Table 3 - Linear paraffins used in this research.....	30
Table 4 - Experimental temperatures. ....	37
Table 5 - Experimental flow rates. ....	37
Table 6 - Determination of the vapor pressure and initial inlet concentration. ....	38
Table 7 - Textural properties of the adsorbents: BET surface area ( $S_{BET}$ ), pore diameter ( $D_{pore}$ ) and total pore volume ( $V_{pore}$ ) [45].....	48
Table 8 - Adsorbents diameter. ....	50
Table 9 - Specific volume. ....	50
Table 10 - Variation of L with flow rate for Fe-PMC1 at different temperatures ( $P_o = 0.0054$ bar of $n-C_7$ ).....	56
Table 11 - Significance of heat effects in ZLC experiments. ....	58
Table 12 - Determination of the saturation time for PMC2. ....	60
Table 13 - Influence of flow rate in kinetic data for PMC1 at 210 °C and $P_o = 0.0054$ bar of $n$ -octane. ....	62
Table 14 - Macropore diffusion data of $n-C_8$ in PMC2 at different temperatures. ....	63
Table 15 - Influence of the sample mass in $n-C_8$ diffusion measurements for PMC1 and Fe-PMC1 at 270 °C and $P_o = 0.0054$ bar. ....	64
Table 16 - Macropore diffusivity of $n-C_7$ in PMC2 at a temperature of 270 °C in different concentrations. ....	66
Table 17 - Diffusion measurements of $n-C_7$ and $n-C_8$ on the AC supports and on Fe-based catalysts supported on AC.....	68
Table 18 - Summary of the diffusion contributions in the effective pore diffusivity.....	71

## ABBREVIATIONS

AC	Activated Carbon
BET	Brunauer-Emmett-Teller
CNT	Carbon Nanotubes
EDS	Energy Dispersive X-Ray Spectroscopy
FID	Flame Ionization Detector
FTS	Fischer-Tropsch Synthesis
GC	Gas Chromatograph
GCMC	Grand Canonical Monte Carlo
IGC	Inverse Gas Chromatography
LT	Long Time
MOF	Metal Organic Framework
MS	Mass Spectrometer
NIST	National Institute of Standards and Technology
NMR	Nuclear Magnetic Resonance
OD	Outer Diameter
PFG	Pulsed Field Gradient
PMC	Polymeric Mesoporous Carbon
PSD	Pore Size Distribution
QENS	Quase Elastic Neutron Scattering
SEM	Scanning Electron Microscopy
ST	Short Time
UFC	Universidade Federal do Ceará
UoE	University of Edinburgh
ZLC	Zero Length Column

## NOMENCLATURE

$a$	External area/volume for a spherical particle
$b$	Langmuir parameter
$c$	Fluid phase concentration of adsorbate
$c_o$	Inlet concentration
$C_s$	Volumetric heat capacity of adsorbent
$D_{app}$	Apparent diffusivity
$D_{ic}$	Intracrystalline diffusivity
$D_p^e$	Macropore diffusivity or effective pore diffusivity
$D_K$	Knudsen diffusivity
$D_m$	Molecular diffusivity
$D_{macro}$	Overall macropore diffusivity
$D_o$	Diffusivity at infinite dilution
$D_{pore}$	Pore diameter
$F$	Purge flow rate
$h$	Heat transfer coefficient
$k$	Boltzmann constant
$K$	Dimensionless Henry constant
$L$	Defined of equation (10) and (19)
$L_{Tr}$	Defined of equation (23)
$m_{ads}$	Sample mass inside the ZLC cell
$M$	Molecular weight of the diffusing species
$Nu$	Nusselt dimensionless number
$P$	Total pressure the system
$P_o$	Partial pressure of the diffusing species
$q$	Adsorbed-phase concentration of adsorbate
$q_o$	Adsorbed amount in equilibrium
$q_s$	Maximum capacity
$\bar{q}$	Value of $q$ averaged over the crystal
$r$	Radial coordinate
$R$	Ideal gas constant
$R_c$	Crystal radius

$Re$	Reynolds dimensionless number
$R_p$	Bead radius
$S_{BET}$	BET surface area
$t$	Time
$T$	Temperature
$T_o$	ZLC working temperature
$V_b$	Volume of the sample holder
$V_f$	Volume of fluid phase inside the ZLC cell
$V_{pore}$	Total pore volume
$V_s$	Adsorbent total volume inside the ZLC cell
$V_{sv}$	Specific volume

#### *Greek Letters*

$\alpha$	Defined of equation (32)
$\delta$	Defined of equation (33)
$\gamma$	Defined of equation (34)
$\lambda$	Nonlinearity parameter
$\beta_n$	Roots of equation (9)
$\beta_{Tr}$	Roots of equation (9) as a function of $L_{Tr}$
$\Delta H_{ads}$	Heat of adsorption
$\varepsilon_p$	Porosity of the particle
$\tau$	Macropore tortuosity
$\varphi$	Thermal conductivity
$\sigma_{12}$	Characteristic length parameter of the binary pair
$\sigma_\infty$	Lower baseline
$\sigma_o$	Upper baseline
$\Omega_{D,12}$	Collision integral

## CONTENTS

1	INTRODUCTION .....	17
1.1	Thesis objectives.....	17
2	LITERATURE REVIEW .....	19
2.1	Fischer-Tropsch Synthesis (FTS).....	19
2.2	Activated carbon (AC) .....	21
2.3	Diffusion mechanisms .....	21
2.3.1	Molecular diffusion.....	23
2.3.2	Knudsen diffusion .....	23
2.4	ZLC historical development.....	24
3	MATERIALS, METHODS AND MODEL .....	29
3.1	Materials.....	29
3.1.1	Adsorbents .....	29
3.1.1.1	Preparation of activated carbon (AC) supports.....	29
3.1.1.2	Preparation of Fe-based catalyst supported on AC.....	30
3.1.2	Hydrocarbons .....	30
3.2	Methods .....	31
3.2.1	Adsorbent Textural Characterization .....	31
3.2.2	Scanning Electron Microscopy couple to Energy Dispersive X-Ray Spectroscopy (SEM-EDS) .....	31
3.2.3	Determination of the specific volume .....	31
3.2.4	<i>Zero Length Column</i> (ZLC) Method.....	32
3.2.4.1	ZLC Data Acquisition.....	35
3.2.4.2	ZLC Experimental Conditions.....	37
3.2.4.3	<i>Zero Length Column</i> (ZLC) Mathematical Model.....	38
4	RESULTS .....	45
4.1	Adsorbent Characterization.....	45

4.2	SEM-EDS.....	48
4.3	Specific volume .....	50
4.4	<i>Zero Length Column</i> (ZLC) experimental results .....	51
4.4.1	Determination of the main diffusion path .....	51
4.4.2	Determination of kinetic control.....	54
4.4.3	Evaluation of heat effects .....	57
4.4.4	Determination of the saturation time .....	58
4.4.5	Influence of the flow rate in the kinetics of adsorption .....	61
4.4.6	Influence of the temperature in the kinetics of adsorption.....	62
4.4.7	Influence of the adsorbent mass in the kinetic data .....	63
4.4.8	Influence of concentration in the kinetic data .....	64
4.4.9	Diffusion of linear paraffins in activated carbons supports and Fe-based catalysts supported on AC .....	67
4.4.9.1	<i>n</i> -heptane and <i>n</i> -octane .....	67
4.4.9.2	<i>n</i> -dodecane .....	68
4.4.10	Analysis of the diffusion process.....	69
5	SUMMARY AND CONCLUSIONS.....	72
	REFERENCES.....	73



## 1 INTRODUCTION

During the last decades, the energy matrix worldwide is changing considerably. According to this scenario, energy companies are performing a considerable effort to develop new energies sources and to improve the old ones. As a consequence, processes involving the Fischer-Tropsch synthesis (FTS) are getting a special attention due to its hydrocarbons products without contaminants.

Despite its consolidation in industrial processes, FTS still has space for improvements associated with novel catalysts. However, the mechanisms occurring in the porous solids still need to be understood.

Among the different catalytic materials used in the FTS, activated carbons are getting a special attention due to its versatility and complexity. However, there is a lack of studies regarding the diffusion measurements of Fischer-Tropsch products on activated carbons in comparison with hydrocarbon diffusion measurements on zeolites, silicas and aluminum oxides.

For that reason, the present work intends to verify mass transfer limitations of the reactants and products of the FTS catalyzed by activated carbon catalysts along with the creation of a database of diffusion measurements to be applied in further studies. The reactants are the components of synthesis gas ( $H_2$ , CO and  $CO_2$ ) and the products are the various hydrocarbons formed, including paraffins corresponding to the range of Diesel ( $C_{8+}$ ), which are of great interest for the Brazilian energy matrix today.

In other words, the structure and chemical nature of the activated carbons carry out a great influence on the kinetics of catalytic route of various hydrocarbons substances involved in the FTS, indicating the need for a better comprehension regarding the mass transport properties to improve the development of materials and processes.

### 1.1 Thesis objectives

After introducing the motivation of this work, this thesis aimed to investigate the diffusion measurements of linear paraffins on activated carbons by the *Zero Length Column* (ZLC) method which is an inexpensive and simple experimental technique. In order to check the consistency of the results, all aspects

that are involved in the ZLC experiments are presented, such as the influence of the temperature, the influence of the dead volume, flow rate and saturation time on the obtained kinetic data. Besides that, adsorbent textural and structural characterizations are provided in order to better understand the kinetics of adsorption.

## 2 LITERATURE REVIEW

This chapter will present the main aspects that influenced the development of this work. Initially, the FTS is briefly described in order to show the relevance of its products (high-value hydrocarbons) taking a special attention in catalysts supported on activated carbons. Next, there will be a short description of the studied porous material, indicating its relevance and application on industrial processes. Then, the fundamentals of diffusion mechanisms are presented in order to provide a better knowledge about the resistances and influences that are on FTS products when they get out from the catalyst. Later, among the different macroscopic and microscopic experimental methods to obtain diffusion values, there is a final section presenting a historical ZLC development, indicating the most important works that supported the obtained results.

### 2.1 Fischer-Tropsch Synthesis (FTS)

The FTS is a potentially attractive technology that converts syngas to high-molecular-weight hydrocarbons [1], which is usually produced from coal or biomass gasification and from the natural gas reform. FTS occurs in metal catalysts (mainly Fe and Co) supported with or without the use of promoters (Cu, Potassium, Mn, etc.) [2, 3] and currently operates in two modes [4] (Table 1).

Table 1 - Operational conditions of FTS.

Processes	Temperature (°C)	Pressure (bar)	Catalysts	Products	Products phase
<i>Low-temperature FTS</i>	200-240	20-40	Iron or Cobalt-based	High molecular mass linear waxes	Liquid
<i>High-temperature FTS</i>	300-350	27-45	Iron-based	Gasoline and linear low molecular mass olefins	Gas

Source: This research.

There is also catalysts based on ruthenium (Ru), however they are usually much more expensive than iron-based catalysts (Fe) or cobalt (Co). Although in many cases, cobalt is preferable to iron due the lower selectivity for the water-gas-

shift reaction [5], the latter has the advantage of being more active at high pressures, less expensive and also may be more adaptable for biomass syngas (mixtures containing CO<sub>2</sub>).

The efficiency of the FTS may be improved through the design of new catalysts leading to a higher conversion of syngas, a higher yield of C<sub>5+</sub> and a lower methane selectivity [6-8]. In the FTS, the catalytic activity and selectivity are influenced by the nature and structure of the support; dispersion and metal charge; and the catalyst preparation method [9]. Many efforts have been made in order to better understand the relationship between the textural properties of the support and the performance of the catalysts developed in its corresponding support [2].

Among the most extensively studied supports, it may be included several types of activated carbons, molecular sieves and simple oxides (Al<sub>2</sub>O<sub>3</sub>, MgO, SiO<sub>2</sub> and TiO<sub>2</sub>) [2, 10]. In the last years, structures known as carbon nanotubes (CNT - Carbon nanotubes) as well as an emerging class of materials known as Metal-Organic Frameworks (MOFs) have been considered as possible new supports for various chemical reactions, including FTS [11-14].

Each class of materials has its advantages over the others. Zeolites, aluminum oxides and mesoporous silicas, such as SBA-15 and MCM-41, are more traditional supports and fairly applied in FTS, which is mainly due to good thermal stability. Most recent studies on the production of catalysts from these materials are dedicated to the analysis of the influence of the promoters, the production method and the dispersion of the catalyst, for example, on the catalytic efficiency [15-19]. On the other hand, the low cost, the known high surface area, large pore size distribution and the complex surface chemistry of the activated carbons (AC) [2, 12] are properties that make these materials very attractive for the development of heterogeneous catalysts, despite their low thermal stability.

The impact of the surface chemistry and support textural properties on the performance of many (and new) catalysts used in FTS is still not fully understood. Besides that, studies on the effect of the size and distribution of the metal (nano) particles either have been proved to be inconsistent or the process remains poorly understood [2, 20], thus it is necessary to better understand the catalysts performance along with the limiting diffusion mechanisms on the FTS products.

## 2.2 Activated carbon (AC)

The importance of activated carbon consists in its versatility because of its high surface area and micropore volume, considering it one of the most complex solids [21].

Activated carbon is a member of a family of carbons ranging from carbon black to carbon fibers but all coming from organic parent sources with different carbonization and manufacturing processes [22]. The term activated carbon (AC) is used to indicate a highly porous material made by thermal decomposition of carbonaceous material followed by a chemical or physical activation [23].

Generally, AC presents a trimodal pore size distribution, but its distribution and the total pore volume are however associated to the pyrolysis and activation initial conditions [24]. Despite their complex pore network, AC has also a complex chemical surface that is associated with its source as well as its activation process [21].

Due to its versatility, AC are widely used in adsorption process, such as the adsorption of organics in decolorizing sugar, water and air purification, separation of gas mixtures and adsorption of gasoline vapors in automobiles [22, 24].

## 2.3 Diffusion mechanisms

Porous solids are generally consisted of microporous crystals into a macropore pellet. Such solids, when evaluating their kinetics of adsorption, present two diffusional resistances to mass transfer: the micropore resistance and the macropore resistance [24].

The basic fundamentals of diffusion can be found in the literature [24-26]. However in this section, only the main diffusional resistances will be described in order to provide a better understanding about the diffusion mechanisms in porous solids without mentioning its governing equations. The governing equations are going to be presented in Chapter 4.

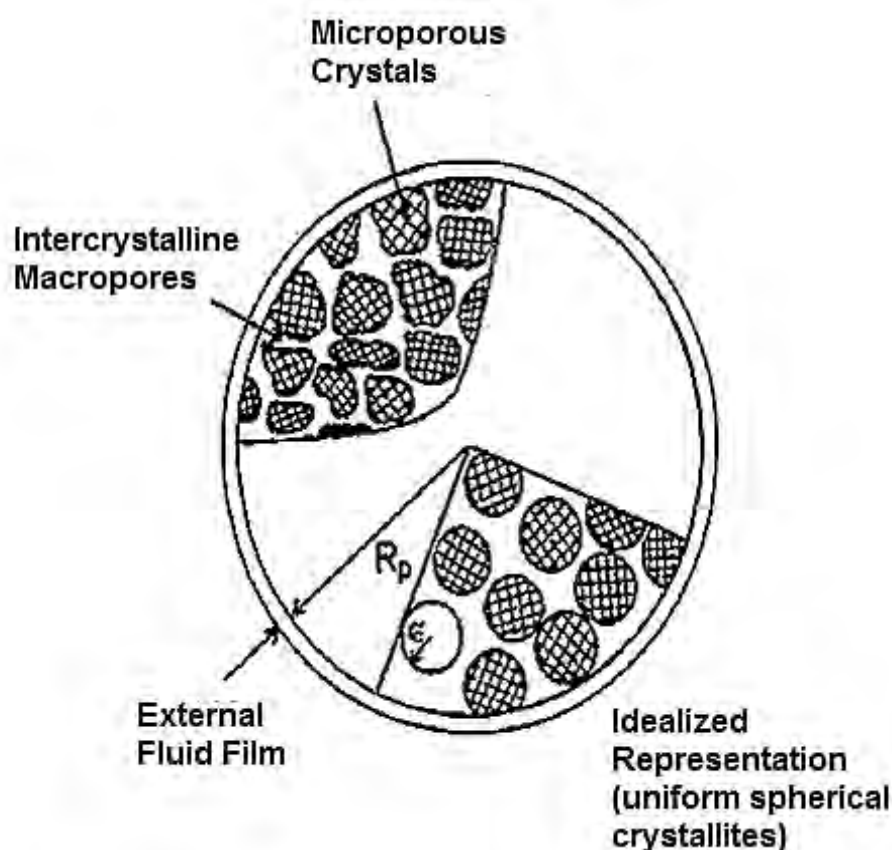


Figure 1 - Main resistances to mass transfer in porous solids [24].

In Figure 1, it is presented the different mechanisms of diffusion by regions of porosity. In the region of microporous crystals (pore diameter  $< 20 \text{ \AA}$ ), the micropore diffusivity or configurational diffusivity or intracrystalline diffusivity is predominant. As a consequence, the diffusion is dominated by interactions between the diffusing molecule and the pore wall [26]. The intracrystalline diffusivity is influenced by steric effects and is considered an activated process. That is, the diffusion mechanism occurs by a sequence of jumps between regions of relatively low potential energy (sites) [26].

Within the macropore region (pore diameter  $> 20 \text{ \AA}$ ), the predominant diffusivities change and the configurational diffusivity do not influence the kinetics measurements. In this region, four distinct mechanisms generally contribute to the macropore diffusion: molecular diffusion, Knudsen diffusion, Poiseuille flow and surface diffusion [24]. Poiseuille flow and surface diffusion are disregarded due to the working operational conditions of this study and their explanation can be found elsewhere [21, 24, 27].

### 2.3.1 Molecular diffusion

According to Ruthven [24], the molecular diffusivity is essentially independent of composition with this type of diffusion becoming significant in large pore sizes and high system pressures; here, molecule-molecule collisions are dominant over the collision between molecules and the wall (Figure 2) and this diffusivity mechanism is dependent of the total pressure and temperature.

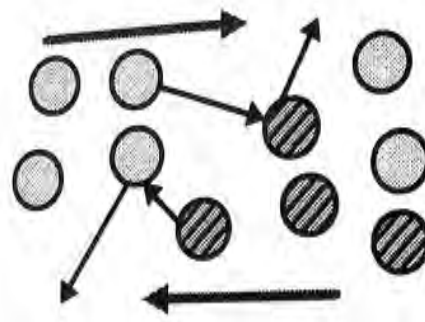


Figure 2 - Molecular diffusion mechanism [21].

Molecular diffusion will be the dominant transport mechanism whenever the mean free path of the gas is small relative to the pore diameter.

### 2.3.2 Knudsen diffusion

Under conditions of low pressure and small pores, the mean free path of the gas is greater than the pore diameter, thus collisions between the molecules and the walls become more relevant than molecule-molecule collisions. The driving force for this transport mechanism is due to molecular collisions and is known as Knudsen diffusion [24].

In such diffusion mechanism, when the molecules strike the pore wall (Figure 3), they are instantaneously adsorbed and re-emitted in a random direction. The direction in which the molecules are emitted has no relation to its original direction before the collision and it is this randomness that characterizes this diffusion process [24].

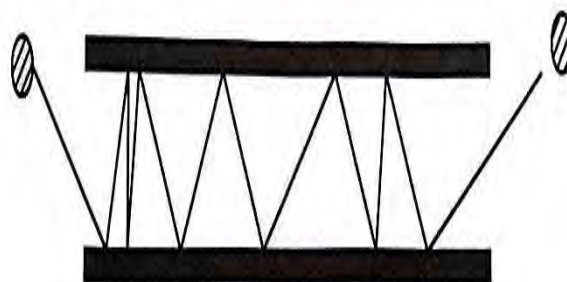


Figure 3 - Knudsen diffusion mechanism [21].

The Knudsen flux depends mainly on the molecular weight of the diffusing species. Thus, lighter molecules travel faster than the ones with high molecular weight under the same concentration gradient. With this mechanism, it is possible to separate mixtures [21].

## 2.4 ZLC historical development

Currently, there are several methods to measure molecular migration in porous solids, both at microscopic and macroscopic level.

In general, microscopic methods should be capable to characterize the molecular movement in short intervals of time and distance. It can be pointed out as microscopic method the *Nuclear Magnetic Resonance (NMR) with Pulsed Field Gradient (PFG)* and *Quase Elastic Neutron Scattering (QENS)*.

On the other hand, macroscopic methods are based on investigation of molecular flow behavior of a system subjected to a concentration gradient according to Fick's second law of diffusion. Gravimetric method, Membrane technique, Chromatographic method and the ZLC technique are representative of macroscopic methods.

Among, the different experimental methods to measure diffusivity, in this section, it is presented the historical development of the ZLC technique, indicating the most relevant works (Table 2) that influenced on the understanding of the obtained results.



Table 2 - ZLC historical development.

Year	Paper	Authors
1988	<i>A new experimental technique for measurement of intracrystalline diffusivity</i>	Eic and Ruthven [28]
1993	<i>Theory of zero length column chromatography with the condition of a well-stirred sorbing zone</i>	Micke et al. [29]
1993	<i>Diffusion of oxygen and nitrogen in 5A zeolite crystals and commercial 5A pellets</i>	Ruthven and Xu [30]
1994	<i>Measurement of intracrystalline diffusion by zero length column tracer exchange</i>	Hufton et al. [31]
1995	<i>Adsorption of branched and cyclic paraffins in silicalite. 2. Kinetics</i>	Cavalcante and Ruthven [32]
1995	<i>Analysis of ZLC desorption curves for liquid systems</i>	Brandani and Ruthven [33]
1996	<i>Analysis of ZLC desorption curves for gaseous systems</i>	Brandani and Ruthven [34]
1996	<i>Moments analysis of the Zero Length Column method</i>	Brandani and Ruthven [35]
1996	<i>Analytical solution for ZLC desorption curves with bi-porous adsorbent particles</i>	Brandani [36]
1996	<i>Analysis of ZLC technique of diffusivity measurements in bidisperse porous adsorbent pellets</i>	Silva and Rodrigues [37]
1996	<i>Transport diffusion and self-diffusion of benzene in NaX and CaX zeolite crystals studied by ZLC and tracer ZLC methods</i>	Brandani et al. [38]
1998	<i>Effects of nonlinear equilibrium on zero length column experiments</i>	Brandani [39]
1998	<i>Heat effects in ZLC experiments</i>	Brandani et al. [40]
2000	<i>ZLC measurements under non-linear conditions</i>	Brandani et al. [41]
2012	<i>Sorption and kinetics of CO<sub>2</sub> and CH<sub>4</sub> in binderless beads of 13X zeolite</i>	Silva et al. [42]
2013	<i>Diffusion mechanism of CO<sub>2</sub> in 13X zeolite beads</i>	Hu et al. [43]

Source: This research.

The ZLC technique was first introduced by Eic and Ruthven [28]. The initial purpose of the technique was to retain the basic advantages of the chromatograph method by following the dimensionless desorption curves while eliminating external intrusions to obtain the intracrystalline diffusivity of strong adsorbed species. In order to verify the consistency of the proposed technique, the results were compared with other methodologies, thus indicating good agreement.

When modelling the ZLC response curves, Eic and Ruthven [28] have proposed several assumptions, such as uniform spherical crystals, linear adsorption isotherm, no external mass transfers and isothermal conditions. However, these conditions were not always fulfilled during experiments with different adsorbents and

sorbates, thus being necessary a better comprehension of the parameters that may influence the desorption curves.

To obtain the kinetic data, a dimensionless theoretical curve is matched with the ZLC response curve at longer times, thus providing the intracrystalline diffusivity. Such analysis may contain errors in diffusion measurements due to nonlinear conditions, external mass resistances or wrong baseline selection, for example.

For this reason, Micke et al. [29] proposed a complete solution of the ZLC mathematical model including effects of isotherm non-linearity, external mass transfer and adsorbent shape to obtain the intracrystalline diffusivity. According to the author, the complete ZLC model is well described by Volterra integral equations and predicted the ZLC experimental results satisfactory.

In the same year as the study proposed by Micke et al. [29], Ruthven and Xu [30] studied the diffusion on large crystals of zeolites and verified that in such adsorbents, the intracrystalline diffusivity obtained from the ZLC method is insignificant in the sorption kinetics. For this reason, they developed a model in which macropore diffusion is matched with the dimensionless ZLC response curve, indicating that diffusivity is mainly contributed by molecular diffusion at higher temperatures and surface diffusion at lower temperatures.

In the year after, Hufton et al. [31] developed a variant of the ZLC technique. Instead of obtaining the transport diffusivity, the new technique allowed the measurement of the self-diffusivity. That is, replacing the FID by a mass spectrometer (MS), it was possible to measure desorption curves of different species, at the same time, following their decrease in intensities on the MS.

In order to understand the influence of the adsorbate phase and different hydrocarbon chains (branched, cyclic, linear), continuous efforts have been done to sort out its influence on the ZLC response curves.

First, Cavalcante and Ruthven [32] observed that the diffusion of  $C_6$  paraffins (single-component) in silicalite is faster for linear single-branched than for cyclic paraffins. Then, Brandani and Ruthven [33] analysed the ZLC desorption curves for a liquid-phase adsorption system indicating that in such system, neglect the external fluid-phase hold-up may provide erroneous diffusion measurements.

In addition to the liquid-phase adsorption system, Brandani and Ruthven also analysed the ZLC desorption curves for gaseous systems [34]. In their study

with gaseous system, they proposed the analysis at short time (ST) to obtain kinetic parameters and indicated that the initial portion of the desorption curves is less sensitive to the errors derived from baseline drift or heat dissipations when compared with the long time (LT) analysis. However, a comparison between ST and LT analysis should be carried out to check the validity of the data [34].

Among the different analysis to obtain kinetic data from ZLC desorption curves, Brandani and Ruthven [35] proposed a different technique to obtain intracrystalline diffusivities based on the moment analysis of the desorption curves. This technique was considered useful for desorption curves of strong adsorbed species and extracted relevant parameters using the entire desorption curve [35].

Despite the reliable diffusion data obtained by the ZLC technique, the ZLC modelling assumptions were still being verified. Brandani et al. [38] investigated the intrusion of extracrystalline mass transfer limitations in a series of ZLC experiments changing the sample quantity, crystal size, nature of the carrier gas and sorbate partial pressure and thus verified the consistency between the basic ZLC theory and the experiments.

Other important aspect in which compromises the diffusion measurements may be the isothermal condition. Brandani et al. [40] proposed a simple criterion to verify if thermal effects are negligible. Its study showed that heat effects are generally insignificant in intracrystalline diffusivities, but it can become important in the measurement of macropore diffusivities.

Another assumption when modelling ZLC and which may influence the ZLC parameters is the linear adsorption equilibrium. Sometimes, experiments under this condition need a really low pressure of adsorbate, thus providing experimental signal in the range of detector's error. As a consequence, an increase in the concentration provides a better signal, but may compromise the linear equilibrium assumption when modelling the ZLC.

Therefore, in order to understand the influence of such increase in concentration by comparing with the model proposed by Micke et al. [29], Brandani [39] developed a nonlinear equilibrium model following the Langmuir isotherm. Its study considered the diffusion model concentration dependent, thus verifying that diffusivities values yielded the correct order of magnitude when compared with the linear model. However, if the nonlinear equilibrium conditions are disregarded, it may provide large errors in equilibrium constant by the ZLC model.

To check the consistency of the nonlinear model, a paper of Brandani et al. [41] showed that the analytic approximation provided a good representation of the desorption response curves under nonlinear conditions.

Since industrial processes use adsorbents with wide range of pores and taking into account that the ZLC method was successfully in measuring the intracrystalline diffusivity, Brandani [36] and Silva and Rodrigues [37] proposed theoretical models for ZLC desorption curves identifying the various region of control (micropore diffusion, macropore diffusion) in order to better understand which diffusion path is dominant.

As a consequence of the different controlling diffusion mechanisms in the adsorbents, Silva et al. [42] and Hu et al. [43] investigated the kinetics of dioxide carbon in 13X zeolite beads by the ZLC method in order to evaluate the most dominant diffusion mechanism. Both authors interpreted different diffusion mechanism by the ZLC curves for the same sample.

Finally, the presented papers were the foundation of this work and were the starting point to the comprehension and development of this thesis.

### 3 MATERIALS, METHODS AND MODEL

In this chapter, the preparation of the used materials, as well as the methods applied to obtain their textural and structural characteristics will be discussed. The following subsections will describe the experimental methods applied during the development of this work, including a full description of the *Zero Length Column* (ZLC) mathematical model under linear and nonlinear equilibrium conditions.

#### 3.1 Materials

##### 3.1.1 Adsorbents

The samples consist of two polymeric mesoporous carbons (PMC) provided by Adsor-Tech GmbH (Büchler Group) and two Fe-catalysts prepared from them. The polymer based carbons, named PMC1 and PMC2, presented spherical shape and differ from each other by their surface chemistry, since the later was produced from the first through a partial oxidation process [44]. The iron catalysts Fe-PMC1 and Fe-PMC2 were prepared from the corresponding carbons according to procedure described in the literature [45-47].

##### 3.1.1.1 Preparation of activated carbon (AC) supports

Cross-linked polystyrene was used as precursor for the sample PMC1. The patented synthesis was conducted in two consecutive steps with the polystyrene being previously sieved to the range of 0.3-0.7 mm [48]. First, the polystyrene undergoes a carbonization step in a batch reactor, where volatile compounds can escape. Next, an activation step with steam occurs in order to establish the pore volume by a controlled oxidation process at 900 °C (Figure 4).

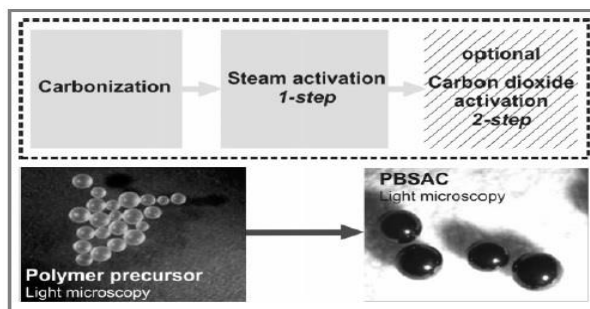


Figure 4 - Schematic production of PMC1 [44].

After producing the PMC1, a part of the sample was then oxidized in air at 200 °C in a batch process producing the PMC2. The oxidation step takes place in order to increase the amount of hydroxyl-, ether-, carboxyl- groups and lactone groups on its surface [49]. With increasing oxidation time, the amount of the mentioned groups increased and turned both activated carbons different in their properties.

### 3.1.1.2 Preparation of Fe-based catalyst supported on AC

Cruz et al. [45-47] described in details the synthesis of Fe-PMC1 and Fe-PMC2 by wet impregnation method followed by a thermal treatment, leading to materials with ca. 50 wt.% load of iron in their structure with an atomic ratio of carbon to iron of  $A_{C:Fe} = 1:1$  [45]. According to the author and its co-workers, these samples were tested as catalysts for Fischer-Tropsch synthesis and produced satisfactory results [45-47].

### 3.1.2 Hydrocarbons

Three linear hydrocarbons (Table 3) of the highest purity were purchased from SIGMA-ALDRICH® and applied in the experiments.

Table 3 - Linear paraffins used in this research.

Compound name	Short name	Purity (%)
<i>n</i> -heptane	<i>n</i> -C <sub>7</sub>	≥99
<i>n</i> -octane	<i>n</i> -C <sub>8</sub>	99
<i>n</i> -dodecane	<i>n</i> -C <sub>12</sub>	≥99

Source: SIGMA-ALDRICH®.

## **3.2 Methods**

### **3.2.1 Adsorbent Textural Characterization**

In order to determine the total pore volume, average pore diameter and specific surface area, nitrogen adsorption-desorption measurements at -196 °C were carried out in a BelSorp (Bel Japan INC., Japan) apparatus. Initially, the samples were degassed for 6 hours at 200 °C under vacuum prior the sorption measurements. From the desorption branch of the isotherms it was possible to obtain the adsorbent textural characteristics [45, 50].

### **3.2.2 Scanning Electron Microscopy couple to Energy Dispersive X-Ray Spectroscopy (SEM-EDS)**

The adsorbents were characterized by SEM-EDS (TES-CAN VEGA XMU) equipped with an EDS BRUKER QUANTAX using an acceleration voltage of 20 kV which provided clear images of the iron catalysts surface as well as their average crystals size and with adequate standards, quantitative analysis of their elemental composition. A more detailed description of the SEM-EDS method and the adsorbents composition is presented in the literature [45-47].

Such analysis along with the N<sub>2</sub> adsorption-desorption isotherms were helpful to understand and evaluate the diffusion mechanism of the hydrocarbons on the studied adsorbents.

### **3.2.3 Determination of the specific volume**

The specific volume of each sample was determined with the aid of a gravimetric apparatus, namely a high-precision magnetic suspension balance (Rubotherm, Germany).

The experimental setup comprises the microbalance, the measuring cell, a data acquisition unit, a thermostat bath, an electric heater and a vacuum pump. The experimental procedure consists of the following steps:

- i) The sample (approx. 1 g) is placed in the measuring cell and is then pre-treated in situ at 150 °C (2 °C/min heating rate) for at least 5 hours under vacuum. The procedure is monitored by recording the sample mass loss, to ensure a constant sample mass, which is an indication of complete sample activation;
- ii) The system is allowed to cool down until the temperature reaches 25 °C.
- iii) With the aid of valves, helium, which is assumed not to adsorb at the working conditions, is allowed into the measuring chamber in order to increase the pressure. The measured sample mass varies until it reaches a stable value, which is then recorded. The gas pressure is increased stepwise and the corresponding mass difference ( $\Delta m$ ) is plotted against the gas density, estimated with an equation of state [51], which provides as the angular coefficient the sum of hanged volumes (under buoyancy effect).

Before those experiments, the volume  $V_b$  of the balance components (i.e. sample holder, hanging wire, etc.) is determined by performing an experiment, as described in step (iii), using no sample and a gas of known density (e.g. nitrogen). The specific volume of the sample,  $V_{sv}$ , is then subtracted from the total volume calculated in step (iii).

#### 3.2.4 Zero Length Column (ZLC) Method

The *Zero Length Column* (ZLC) method is a simple chromatographic technique developed by Eic and Ruthven [28], from insights of previous studies [52], which aimed to determine intracrystalline diffusivity of a wide range of porous materials by following its desorption curves, eliminating heat transfer and extracrystalline mass transfer resistances [28].

A schematic diagram of the ZLC used in this work is presented in Figure 5. The ZLC analysis is conducted in two consecutive steps. First, the samples are saturated with the diffusing species (i.e. the hydrocarbon under analysis) by the contact with a flow of a saturated stream carried by an inert gas ( $N_2$  or He) under controlled temperatures. In the second step, the gas line is switched in order to have



only an inlet of carrier gas, which should purge the diffusing species from the adsorbent due to the generated concentration gradient.

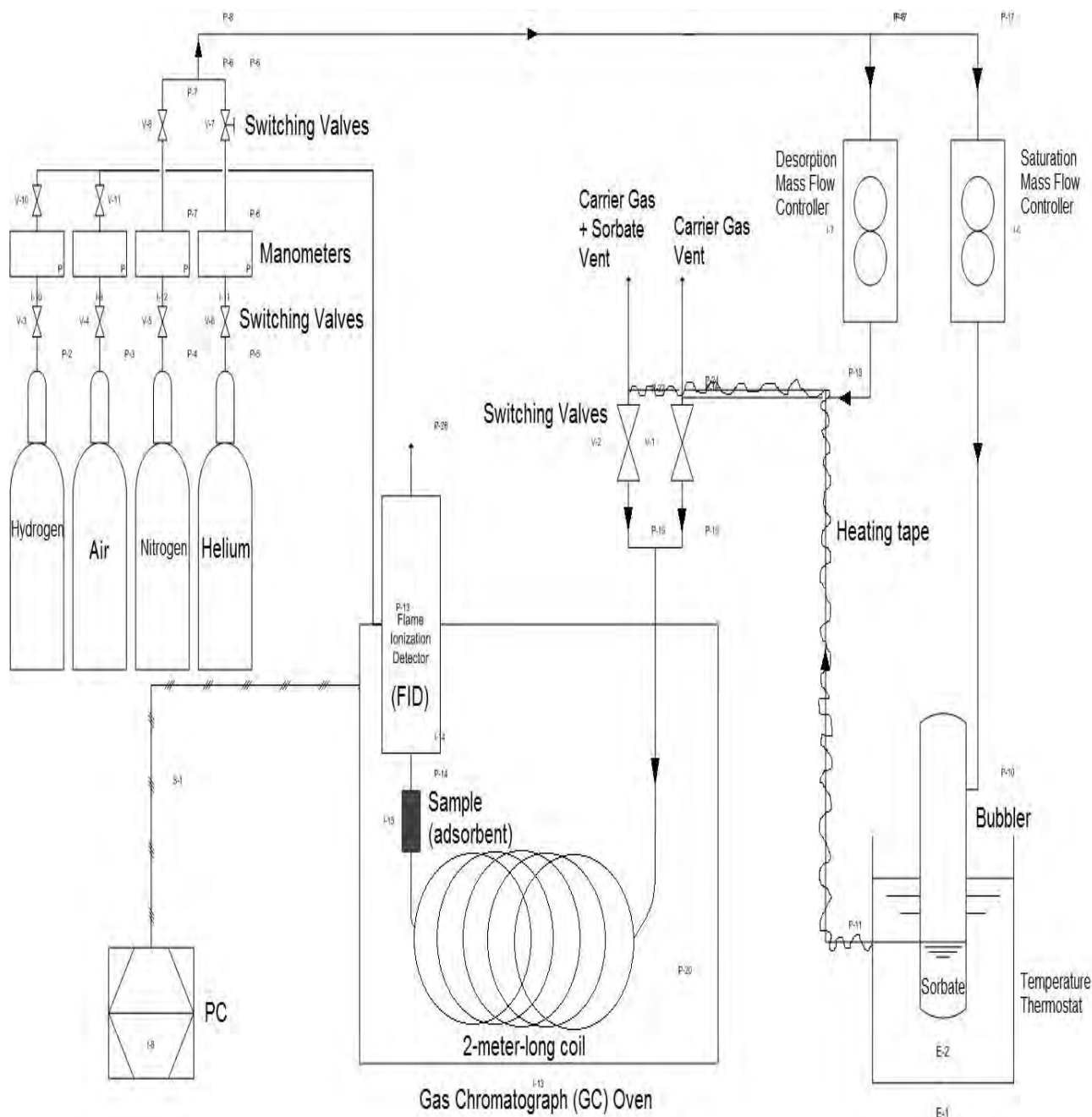


Figure 5 - ZLC Scheme.

The saturated stream is prepared by flowing the carrier gas (inert) through a bubbler containing the hydrocarbon placed in a thermal bath (Julabo F-32 MA). In the outlet of the bubbler (Figure 5), a heating tape at 90-110 °C covers the tube line in order to eliminate any surface condensation in the tubing. To maintain the streams at steady flow rates, mass flow controllers (Matheson, 8170) were used.



Figure 6 - ZLC Apparatus.

Inside the gas chromatograph (GC) oven (Varian, CP-3380), a 2 m-length coil {1/16" outer diameter (OD) SS tube} is connected to the switching valves in order to provide sufficient heat transfer and guarantee that the system will be under isothermal conditions. The ZLC system (Figure 6) has a dead volume of 2.66 cm<sup>3</sup> and operates at turbulent flow regime ( $Re > 4000$ ).

A small amount of adsorbent, generally between 1-5 mg, is placed between two sintered discs acting as flow distributors in an 1/8" SS straight union (right-side of Figure 7) connected vertically to an 1/8" OD SS tube (Figure 8) inside the GC oven with a Flame Ionization Detector (FID) attached after the ZLC Column.

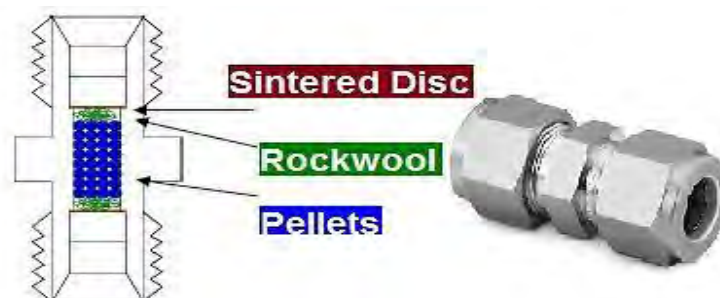


Figure 7 - ZLC Column.

The packed ZLC column is presented in Figure 7 (left-side). Besides the adsorbent, the ZLC column is filled with non-adsorbing rock wool and sealed with sintered discs. The non-adsorbing rock wool is used in order to prevent adsorbents, which may deteriorate during the tests, from blocking the discs and to avoid gas bypass [43].

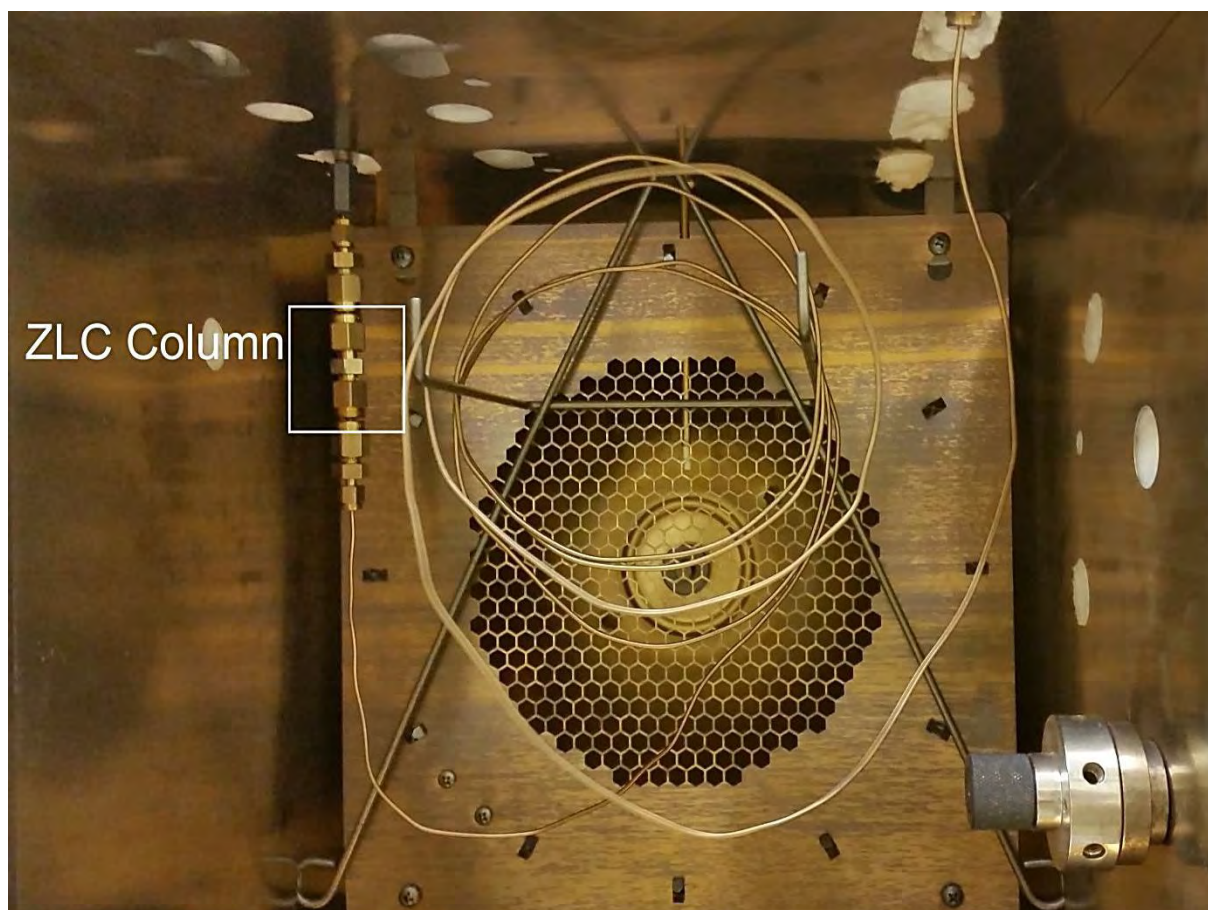


Figure 8 - ZLC Column placed in the system.

Prior to each experimental run, the materials are regenerated by heating them under a helium stream from 25 °C to 290 °C over a period of 10-12 hours at a low flow of helium carrier gas to avoid any water or volatile compounds adsorption, which may compromise the experimental response curve of the ZLC experiments.

#### 3.2.4.1 ZLC Data Acquisition

The resulting output from the ZLC experiment is generally an electric signal, in millivolts, acquired by time, in second (Figure 9). However, it is necessary

to normalize the signal in order to obtain the dimensionless concentration of the adsorbate.

To normalize the desorption experiment it is necessary to determine the baseline signal values. After defining the baselines and applying equation (1), it is possible to plot the desorption curves (Figure 10) verifying the influence of different conditions in the results.

$$\frac{c(t)}{c_0} = \frac{\sigma(t) - \sigma_{\infty}}{\sigma_0 - \sigma_{\infty}} \quad (1)$$

Equation (1) has the upper baseline ( $\sigma_0$ ) which is the average of thirty points of the signal at saturation level before starting the desorption and the lower baseline ( $\sigma_{\infty}$ ) which is the last value of the signal when desorption has ended.

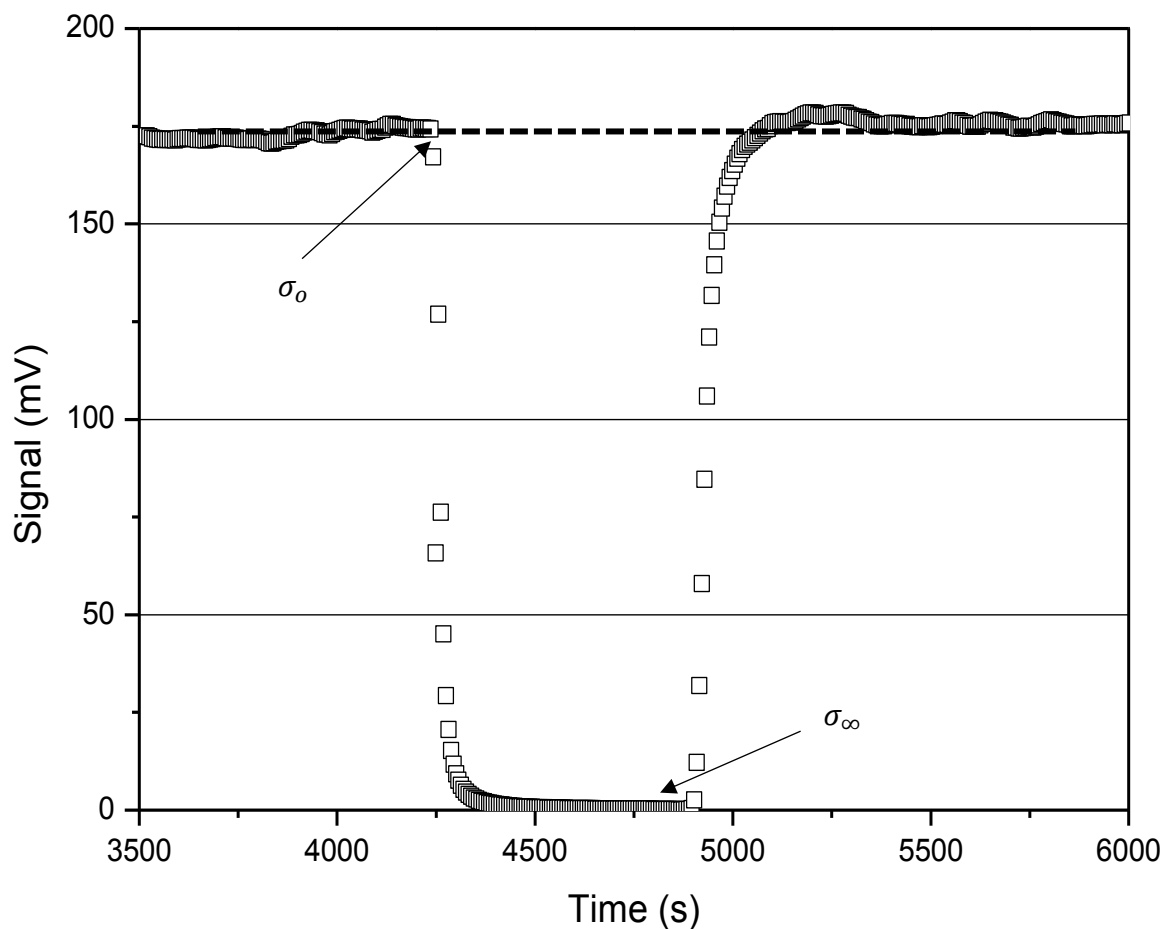


Figure 9 - ZLC experimental signal showing the upper ( $\sigma_0$ ) and lower ( $\sigma_{\infty}$ ) baselines.

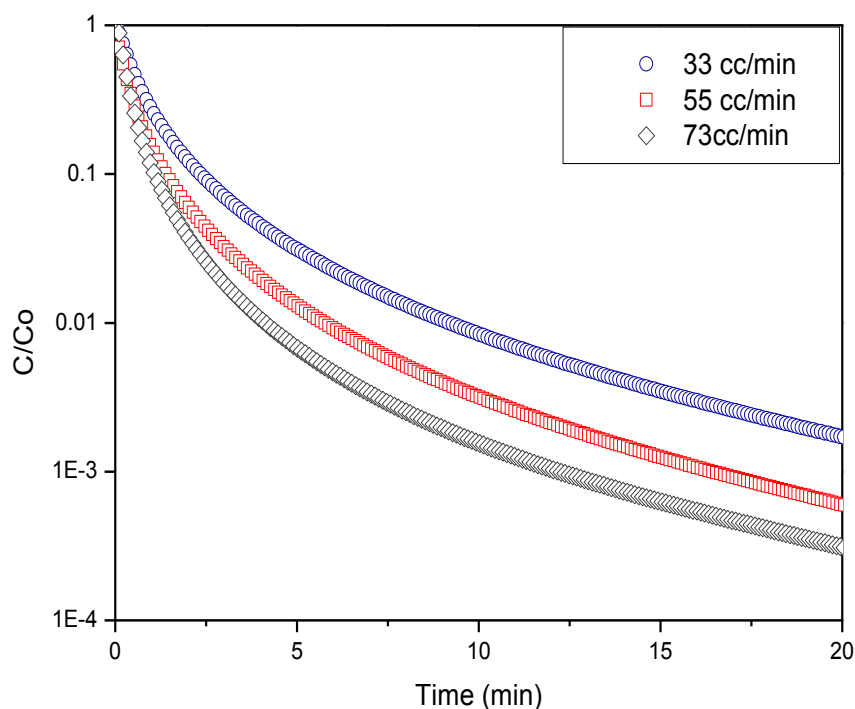


Figure 10 - Plot of normalized concentration versus time.

### 3.2.4.2 ZLC Experimental Conditions

The set of ZLC experiments were carried out at temperatures ranging from 210 °C to 270 °C (Table 4), under three different helium flow rates in the range of 36-73 cc/min (Table 5) with an initial inlet linear paraffin partial pressure of 0.0054 bar for all adsorbents. The helium flow rates were checked with a soap bubbler in the outlet of the system at each experimental temperature.

Table 4 - Experimental temperatures.

Temperature (°C)
210
240
270

Source: This research.

Table 5 - Experimental flow rates.

Flow rate (cc/min)
33
55
73

Source: This research.

The hydrocarbon partial pressure was determined according to the temperature set in the thermostat bath using the vapor tables of the *National Institute of Standards and Technology* (NIST) [53]. Table 6 presents the bath temperatures used for each *n*-paraffin.

Table 6 - Determination of the vapor pressure and initial inlet concentration.

Hydrocarbon	Bath Thermostat Temperature (°C)	Vapor Pressure (bar)	Initial Concentration (mol cm <sup>-3</sup> ) <sup>a</sup>
<i>n</i> -heptane	-15.68	0.00542	2.53E-7
<i>n</i> -octane	5.00	0.00542	2.34E-7
<i>n</i> -dodecane	74.51	0.00542	1.88E-7

<sup>a</sup> - Concentration = P/RT; R = 8.31E-2 L bar K<sup>-1</sup> mol<sup>-1</sup>

Source: This research.

This set of conditions was chosen because they are similar to those used in the Fischer-Tropsch reactions (Table 1) being possible to evaluate correctly the products (*n*-paraffins) diffusion.

### 3.2.4.3 Zero Length Column (ZLC) Mathematical Model

#### Mathematical Modelling of Micropore Diffusion at Linear Equilibrium Conditions

The principle of the ZLC technique consists in obtaining adsorption kinetic data by matching the experimental response curve to the dimensionless theoretical curve derived from the appropriate solution of the Fickian equation of diffusion.

The model of a ZLC system assumes that the column is sufficiently short so that the cell presents no axial gradients, which allows the system to behave as a perfectly mixed cell (Figure 11).

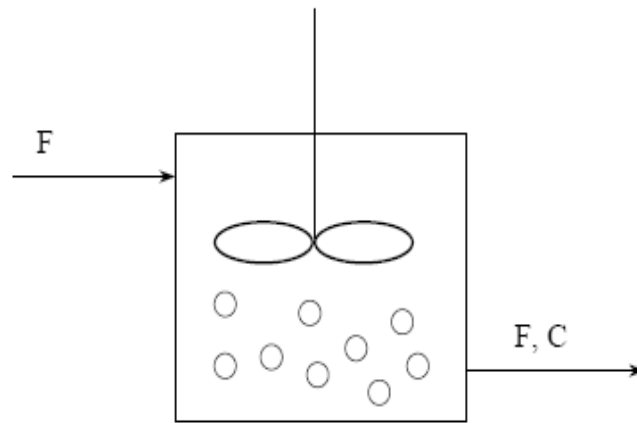


Figure 11 - Perfectly mixed cell.

Therefore, considering (i) an isothermal system of uniform spherical particles with (ii) a linear adsorption equilibrium isotherm at the particle surface and (iii) neglecting the external diffusion resistances, the system may be described by the following set of equations:

Fluid-phase mass balance:

$$V_s \frac{d\bar{q}}{dt} + V_f \frac{dc}{dt} + F \cdot c = 0 \quad (2)$$

Solid-phase mass balance:

$$\frac{\partial q}{\partial t} = D_{ic} \left( \frac{\partial^2 q}{\partial r^2} + \frac{2}{r} \frac{\partial q}{\partial r} \right) \quad (3)$$

and from an overall mass balance in the solid the following relationship holds:

$$\frac{4}{3} \pi R_c^3 \frac{d\bar{q}}{dt} = 4\pi R_c^2 D_{ic} \left( \frac{\partial q}{\partial r} \right)_{r=R_c} \quad (4)$$

Where  $V_s$  is the adsorbent total volume inside the ZLC cell;  $V_f$  is the volume of fluid phase inside the ZLC cell,  $F$  the purge flow rate;  $D_{ic}$  is the intracrystalline diffusivity;  $r$  is the radial coordinate;  $R_c$  is the crystal radius;  $q$  is the

adsorbed-phase concentration of adsorbate;  $c$  is the fluid phase concentration of adsorbate;  $\bar{q}$  is the value of  $q$  averaged over the crystal; and  $t$  the time.

The ZLC system used in this work is a case of gaseous system and in such system, to neglect the accumulation in the fluid phase ( $V_f \cdot dc/dt$ ) is generally a valid approximation due to the low molecular density [54].

The initial and boundary conditions of equations (2) and (3) are:

$$q(r, 0) = q_o = K \cdot c_o \quad (5)$$

$$q(R_c, t) = K \cdot c \quad (6)$$

$$\frac{\partial q}{\partial r}(0, t) = 0 \quad (7)$$

In the initial conditions  $c_o$  is the inlet concentration;  $q_o$  is the adsorbed amount in equilibrium with the initial concentration;  $K$  is the dimensionless Henry constant.

Equation (2) can be considered as a boundary condition on the solid-phase mass balance {eq. (3)} and can then be rewritten as:

$$D_{ic} \frac{\partial q}{\partial t}(R_c, t) + \frac{1}{3} \frac{FR_c}{KV_s} q(R_c, t) = 0 \quad (8)$$

The resulting expression for the desorption curve can be readily obtained from separation of variables or from the problem of diffusion in a sphere with surface evaporation [55].

Expressing in terms of the effluent concentration, the resulting solution is given by:

$$\frac{c}{c_o} = 2L \sum_{n=1}^{\infty} \frac{\exp\left(-\frac{\beta_n^2 D_{ic} t}{R_c^2}\right)}{[\beta_n^2 + L(L-1)]} \quad (9)$$

where  $\beta_n$  is given by the roots of the auxiliary equation:

$$\beta_n \cot \beta_n + L - 1 = 0 \quad (10)$$



and

$$L = \frac{1}{3} \frac{FR_c^2}{KV_s D_{ic}} \quad (11)$$

At longer times (LT), equation (9) reduces to a simple exponential decay curve since only the first term of the series is significant.

$$\frac{c}{c_o} = \frac{2L}{[\beta_1^2 + L(L-1)]} \exp\left(-\frac{\beta_1^2 D_{ic} t}{R_c^2}\right) \quad (12)$$

There is a corresponding expression for desorption curves in one-dimensional model or parallel sided adsorbent slab [34, 56]. However, in this work only the spherical model is suitable.

### Mathematical Modelling of Micropore Diffusion at Nonlinear Equilibrium Conditions

The basic ZLC modelling assumes linear equilibrium conditions at the surface of the adsorbent, i.e. in the Henry's law region. Generally for strongly adsorbed species, conditions of linearity may not be achieved, which may provide a misinterpretation of the experimental results due to limitations in the detector's signal range. In these situations, increasing the initial concentration beyond the linear region is one alternative and is useful to analyse the effect of nonlinearity on the resulting apparent diffusivities ( $D_{app}$ ) [39, 41]

In order to model such system, Brandani [39] took into account a nonlinear equilibrium based on a Langmuir adsorption isotherm {equation (13)} and assumed that the concentration dependence of the diffusivity may be described according to Darken's equation {equation (14)}.

$$\frac{q(r,t)}{q_s} = \frac{bc}{1+bc} \quad (13)$$

$$D(q) = \frac{D_o}{1 - q/q_s} \quad (14)$$

Where  $b$  is the Langmuir parameter;  $D_o$  is the diffusivity at infinite dilution and  $q_s$  is the maximum capacity. The cell mass balance and the solid phase mass balance follow the governing equations (2), (3) and (4) with the resulting dimensionless equations for the nonlinear ZLC model being presented below:

$$\frac{1-\lambda+\lambda C}{1-\lambda} \left( \frac{\partial Q}{\partial \xi} \right)_{\xi=1} + \frac{LC}{1-\lambda} = 0 \quad (15)$$

$$\left( \frac{\partial Q}{\partial \tau} \right) = \frac{1}{1-\lambda Q} \left( \frac{\partial^2 Q}{\partial \xi^2} + \frac{2}{\xi} \frac{\partial Q}{\partial \xi} \right) + \frac{\lambda}{(1-\lambda Q)^2} \left( \frac{\partial Q}{\partial \xi} \right)^2 = 0 \quad (16)$$

The full solution model is obtained by satisfying the initial and the boundary conditions, which are given by:

$$Q = 1 \quad (17)$$

$$Q(1, \tau) = \frac{C}{1-\lambda+\lambda C} \quad (18)$$

$$\left( \frac{\partial Q}{\partial \xi} \right)_{\xi=0} = 0 \quad (19)$$

where the dimensionless parameters are defined as:

$$L = \frac{1}{3} \frac{FR_c^2}{KV_s D_o} \quad (20)$$

$$\lambda = \frac{q_o}{q_s} \quad (21)$$

where  $\lambda$  is the nonlinearity parameter and  $R_c$  is the crystal radius with the dimensionless variables being given by the following set of equations:

$$Q = \frac{q}{q_o} \quad C = \frac{c}{c_o}; \quad \tau = \frac{D_o t}{R_c^2}; \quad \xi = \frac{r}{R_c} \quad (22)$$

In the long time region the following analytic approximation for nonlinear equilibrium conditions that satisfies the long-time asymptote is [39]:

$$\ln\left(\frac{c}{c_0}\right) = \frac{1}{2} \left[ \ln(1 - \lambda) - \lambda + \ln\left\{\frac{2L_{Tr}}{\beta_{Tr}^2 + L_{Tr}(L_{Tr}-1)}\right\} + \ln\left\{\frac{2L}{\beta_1^2 + L(L-1)}\right\} - \beta_1^2 \tau \right] \quad (23)$$

where  $\beta_{Tr}$  is the first root of the auxiliary {eq. (10)} and:

$$L_{Tr} = \frac{L}{(1-\lambda)} \quad (24)$$

where  $L_{Tr}$  is the intercept of a LT asymptote in the case of a tracer exchange [39].

### Mathematical Modelling of Macropore Diffusion

The mathematical modelling for macropore diffusion derived from the ZLC desorption curve is obtained from the particle effective diffusivity or macropore diffusivity [43]:

$$(1 - \varepsilon_p) \frac{\partial q}{\partial t} + \varepsilon_p \frac{\partial c}{\partial t} = \frac{\varepsilon_p}{\tau} D_{macro} \frac{\partial^2 c}{\partial z^2} \quad (25)$$

where  $D_{macro}$  is the overall macropore diffusivity;  $\varepsilon_p$  is the porosity of the particle;  $\tau$  is the tortuosity of the macropores.

In such modelling, the adsorbed phase in the micropores is at linear equilibrium with the gas phase in the macropores, i.e.  $q = K \cdot c$ . Thus, equation (25) can be rewritten as:

$$\{(1 - \varepsilon_p)K + \varepsilon_p\} \frac{\partial c}{\partial t} = \frac{\varepsilon_p}{\tau} D_{macro} \frac{\partial^2 c}{\partial z^2} \quad (26)$$

Therefore, equation (26) can be rearranged to obtain the Fick's diffusion equation and the effective pore diffusivity or the macropore diffusivity ( $D_p^e$ ).

$$\frac{\partial c}{\partial t} = D_p^e \frac{\partial^2 c}{\partial z^2} \quad (27)$$

$$D_p^e = \frac{\varepsilon_p D_{Macro} / \tau}{\varepsilon_p + (1 - \varepsilon_p) K} \quad (28)$$

where the denominator in equation (28) represents the effective bead Henry law constant.

## 4 RESULTS

In this chapter, an overview of the different aspects involved in the ZLC experiments are presented, such as the influence of the temperature, the influence of the dead volume, flow rate and saturation time on the obtained kinetic data, as well as the comparison between the diffusivity data when the adsorbate is changed or when the amount of adsorbent is varied. Additionally, textural properties along with SEM-EDS microphotographs previously measured and published [45] are briefly presented in order to better understand the hydrocarbons diffusional behavior in the studied porous solids.

### 4.1 Adsorbent Characterization

Pore morphology of the studied adsorbents has been previously investigated [45] by measuring nitrogen physisorption isotherms. The isotherm shape provides preliminary information about pore structure [57], which will be useful for the analysis of the kinetic data.

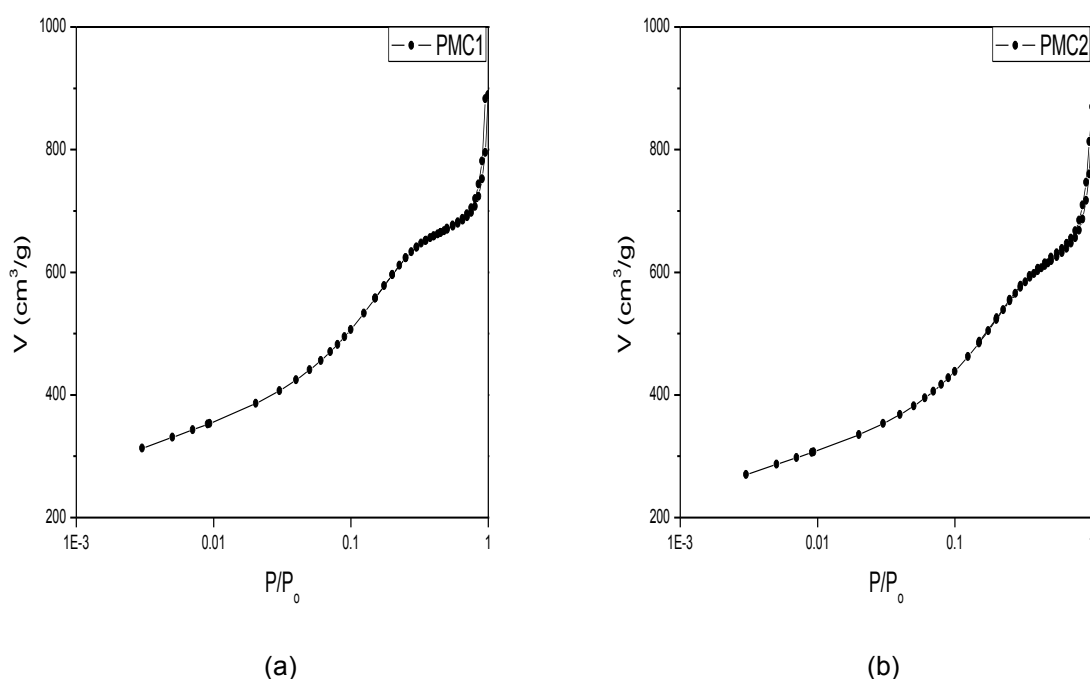


Figure 12 - N<sub>2</sub> adsorption-desorption isotherms of: (a) PMC1; (b) PMC2 [45].

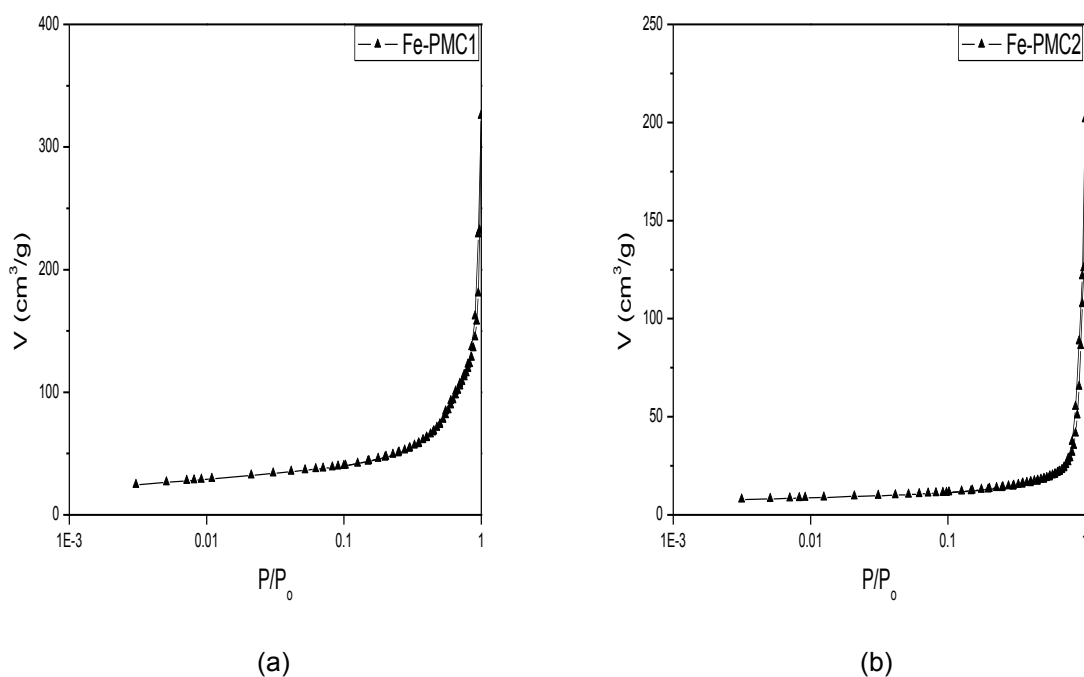


Figure 13 -  $N_2$  adsorption-desorption isotherms of: (a) Fe-PMC1; (b) Fe-PMC2 [45].

According to Cruz et al. [45], PMC1 and PMC2 isotherms (Figure 12) are in accordance with isotherm type IIb with type H4 loop which is characteristic of an activated carbon isotherm [58] whereas the iron catalysts isotherms (Figure 13), are still of type IIb but with a H3 loop. Hysteresis might be related to the presence of mesoporous structure or inter-particle capillary condensation [24, 45, 58].

Monte Carlo calculations [59, 60] were applied to determine the pore size distribution (PSD) of the samples from the  $N_2$  isotherms. The PSD was obtained following the procedure proposed by Davies et al. [60] and Lucena et al. [61] with the results being presented in Figure 14 and Figure 15.

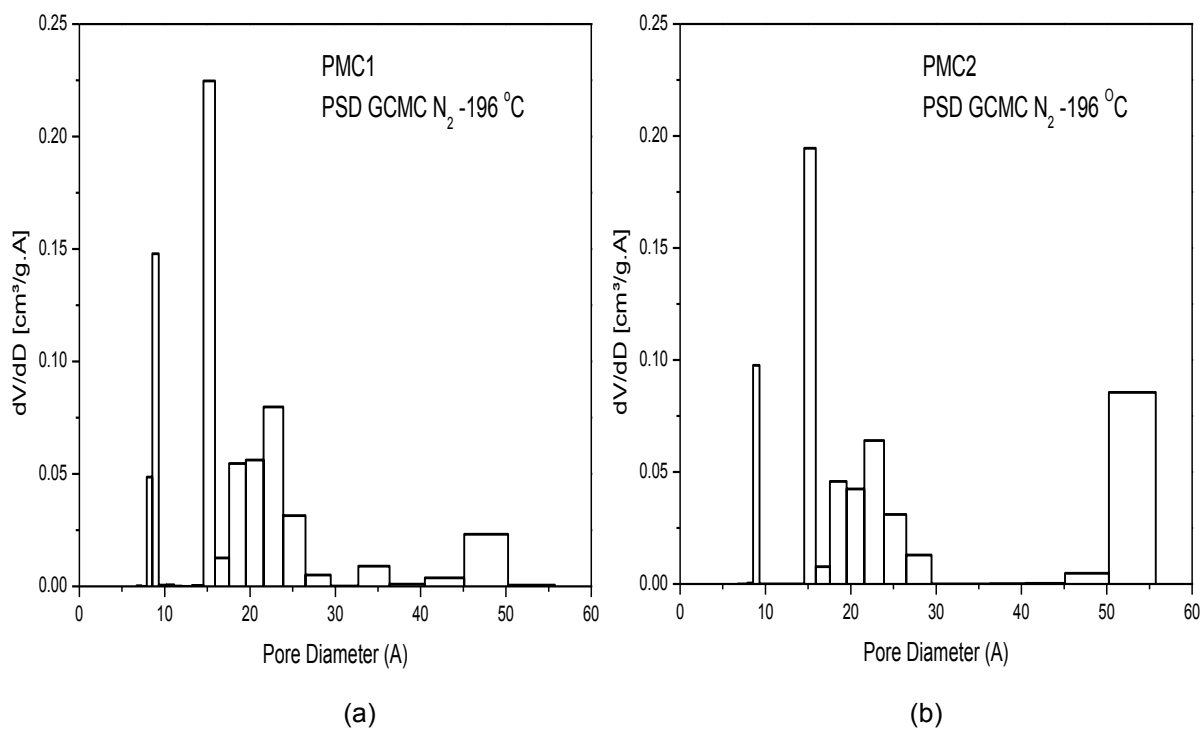


Figure 14 - Pore size distribution of the supports: (a) PMC1; (b) PMC2. GCMC = grand canonical Monte Carlo calculations [45].

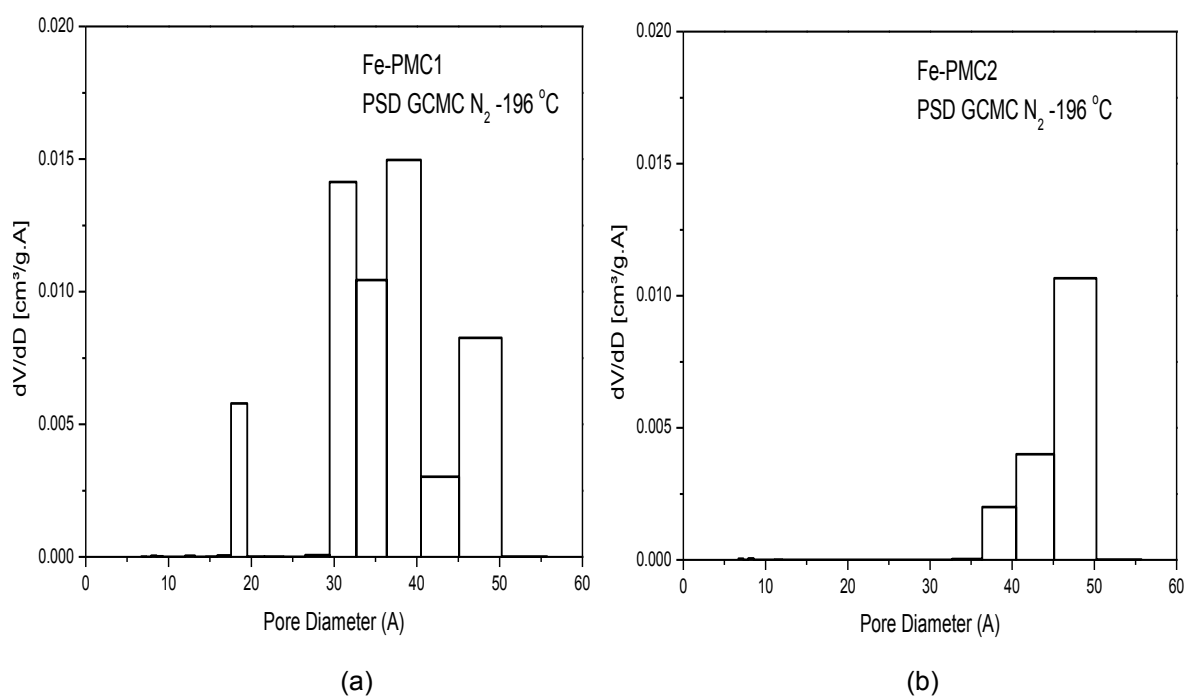


Figure 15 - Pore size distribution of the catalysts: (a) Fe-PMC1 and (b) Fe-PMC2. GCMC = grand canonical Monte Carlo calculations [45].

The wide range of pore sizes shown in Figure 14(a) and Figure 14(b) are in accordance with typical characteristics of activated carbons with bimodal (micro and meso) pore size distribution [21, 24].

After the addition of iron on activated carbon supports, relevant changes in the textural properties were observed, as shown in Table 7. Such a behavior was attributed to a change in the structure of the supports after the wet impregnation and thermal treatment, indicating the formation of aggregated or agglomerated particles that formed pores with non-uniform size and shape [45].

Table 7 - Textural properties of the adsorbents: BET surface area ( $S_{BET}$ ), pore diameter ( $D_{pore}$ ) and total pore volume ( $V_{pore}$ ) [45].

	$S_{BET}$ ( $\text{m}^2 \text{g}^{-1}$ )	$D_{pore}$ (nm)	$V_{pore}$ ( $\text{cm}^3 \text{g}^{-1}$ )
<i>Supports</i>			
PMC1	2070	2.6	1.28
PMC2	1937	2.8	1.37
<i>Catalysts</i>			
Fe-PMC1	147	2.4	0.23
Fe-PMC2	34	1.7	0.11

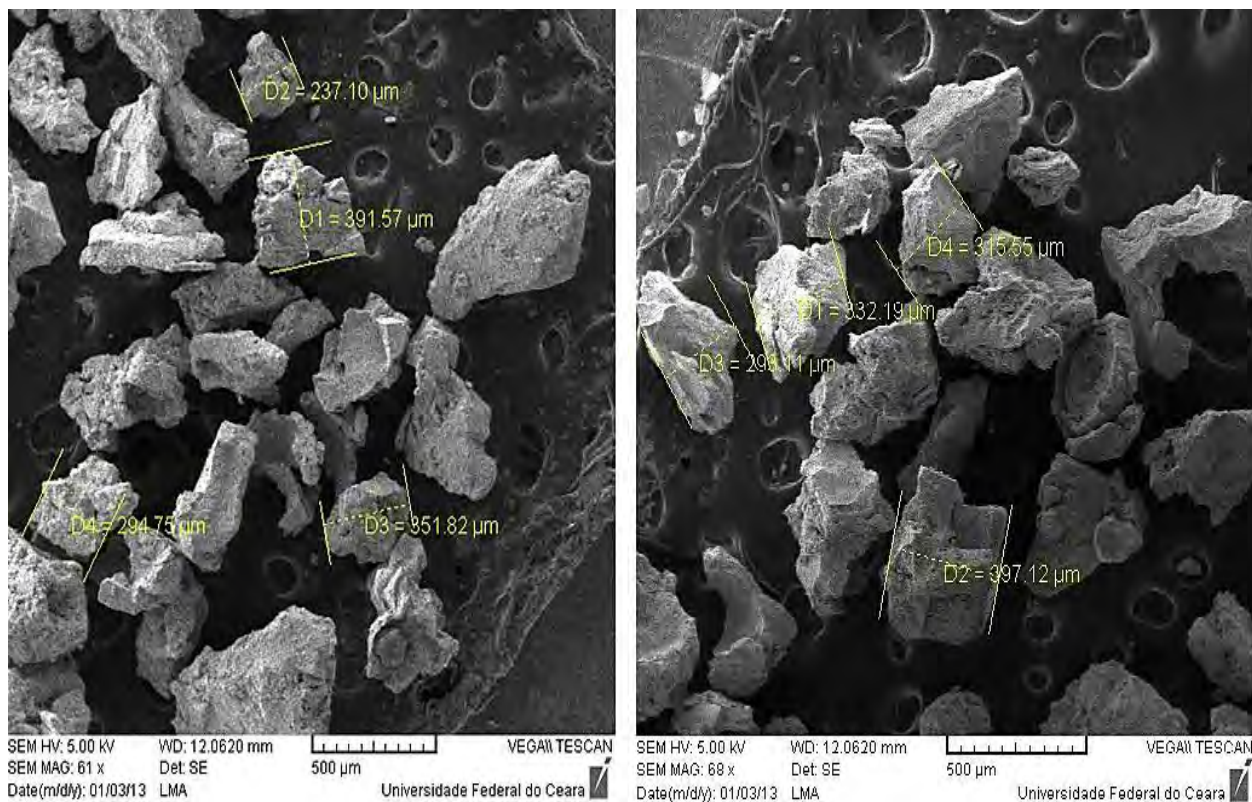
Source: Cruz et al. [45].

## 4.2 SEM-EDS

The morphological aspects concerning the impregnation of iron on the carbon support were evaluated by SEM-EDS. After the wet impregnation and thermal treatment, the iron-based catalysts consisted in globular-like crystals bearing an agglomeration of spherulites [45], as illustrated in Figure 16 and Figure 17. These microphotographs were useful to determine the average diameter of the iron based catalysts.

Along with the nitrogen isotherms, the SEM microphotographs gave an insight in understanding the influence of the iron impregnation on the activated carbon supports. The deposal of iron on the activated carbon structure promoted a decrease in the adsorbents diameter ( $D_{ads}$ ) (Table 8) due to the partial collapse of the solid structure caused by agglomeration of bulk phase on outer surface or on the mouth of the support pores [45]. The resulting catalysts diameter corresponds to an average of the crystals diameter obtained from the SEM microphotographs.

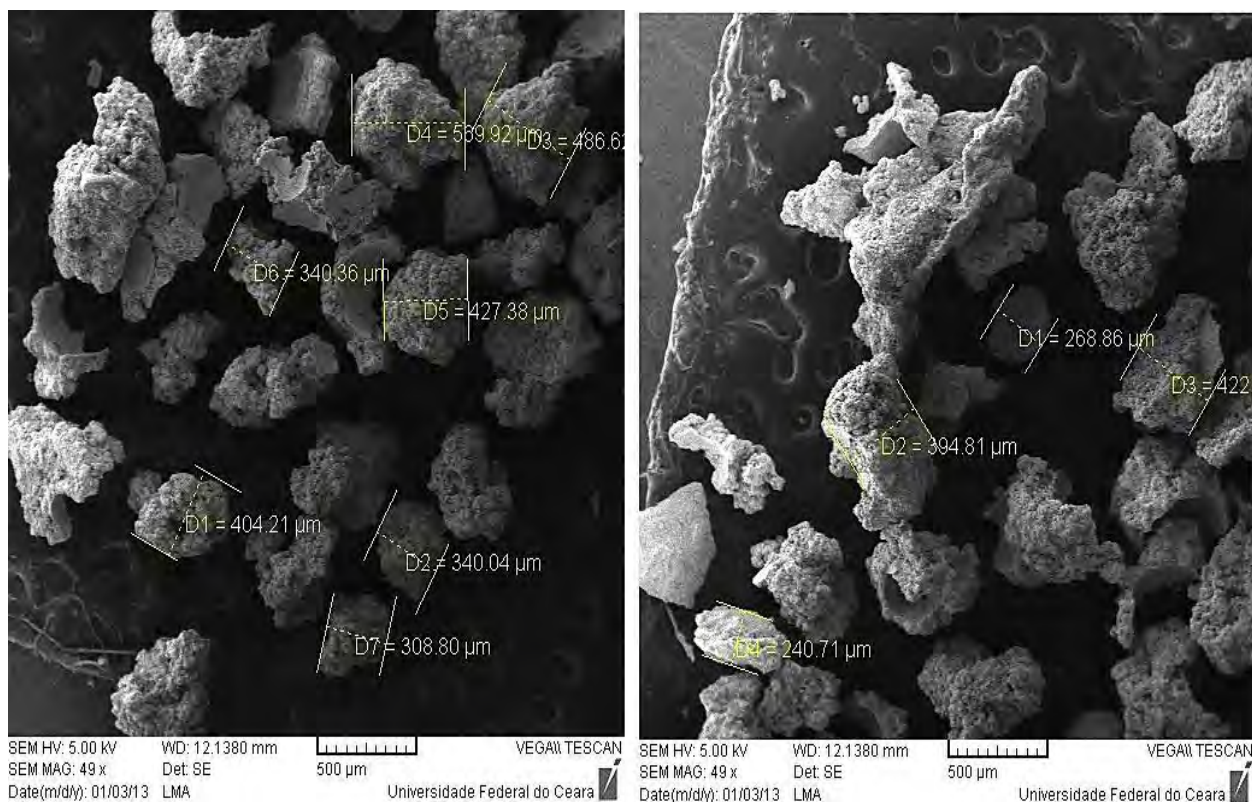




(a)

(b)

Figure 16 - SEM microphotographs of Fe-PMC1.



(a)

(b)

Figure 17 - SEM microphotographs of Fe-PMC2.

Table 8 - Adsorbents diameter.

	$D_{ads}$ (mm)
<i>Supports</i>	
PMC1	0.5*
PMC2	0.45*
<i>Catalysts</i>	
Fe-PMC1	0.352
Fe-PMC2	0.394

Source: This research/\*Adsor-Tech GmbH.

Further morphological aspects and properties regarding the impregnation of iron on the supports, e.g. particle distribution and chemical composition, have been discussed in details by Cruz et al. [45].

### 4.3 Specific volume

The specific volume of each adsorbent is presented in Table 9.

Table 9 - Specific volume.

	$V_{sv}$ (cm <sup>3</sup> g <sup>-1</sup> )	Porosity ( $\epsilon_p$ )
<i>Supports</i>		
PMC1	0.41	0.76
PMC2	0.387	0.78
<i>Catalysts</i>		
Fe-PMC1	0.224	0.51
Fe-PMC2	0.224	0.33

Source: This research.

The specific volume along with the pore volume obtained from the nitrogen physisorption measurements provided the porosity of each adsorbent ( $\epsilon_p$ ) [62].

$$\epsilon_p = \frac{V_{pore}}{V_{sv} + V_{pore}} \quad (29)$$

#### 4.4 Zero Length Column (ZLC) experimental results

The experiments carried out in the ZLC are presented in this section including a parametric analysis of the effects on desorption curves, e.g. saturation time, adsorbent mass, temperature, inert purge flow and adsorbate concentration.

##### 4.4.1 Determination of the main diffusion path

In order to evaluate the predominant mass transfer mechanism occurring in the solids, a set of experiments were run under nitrogen and helium flows. According to Hu et al. [43], when desorption curves from different inert carriers do not overlap, there is an indication of macropore diffusion controlling the desorption process. Otherwise, if the desorption curves overlap under similar conditions with different purge gases, the system is controlled by intracrystalline diffusion [28].

From Figure 18 and Figure 19, corresponding to PMC1 and Fe-PMC1, respectively, it is possible to observe that the desorption curves from He and N<sub>2</sub> do not overlap and present a clear discrepancy in the long time asymptote. This desorption behavior indicates macropore diffusion control and is also observed for PMC2 and Fe-PMC2 (Figure 20 and Figure 21, respectively).

For a macropore-controlled system, the macropore reciprocal diffusional time constant derived from the ZLC desorption curves represents  $D_p^e/R_p^2$  {based on the bead radius ( $R_p$ )} rather than the micropore reciprocal diffusional time constant  $D_{ic}^2/R_c^2$  (based on the crystal radius) [30, 43].

Macropore diffusion control can be also observed when different bead sizes are used [30, 43]. However, in this work only the analysis with different carrier gases was applied.

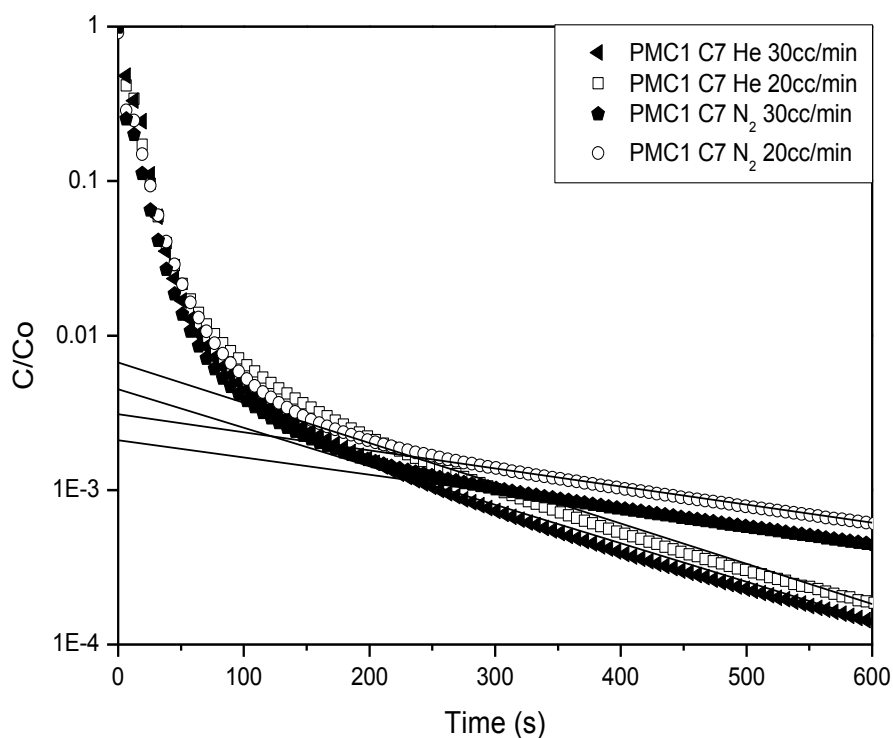


Figure 18 - Comparison of experimental ZLC response curves of PMC1 at  $P_0 = 0.0054$  bar of  $n-C_7$  in two different purge gas (He and N<sub>2</sub>), 270 °C, 20 and 30 cc/min.

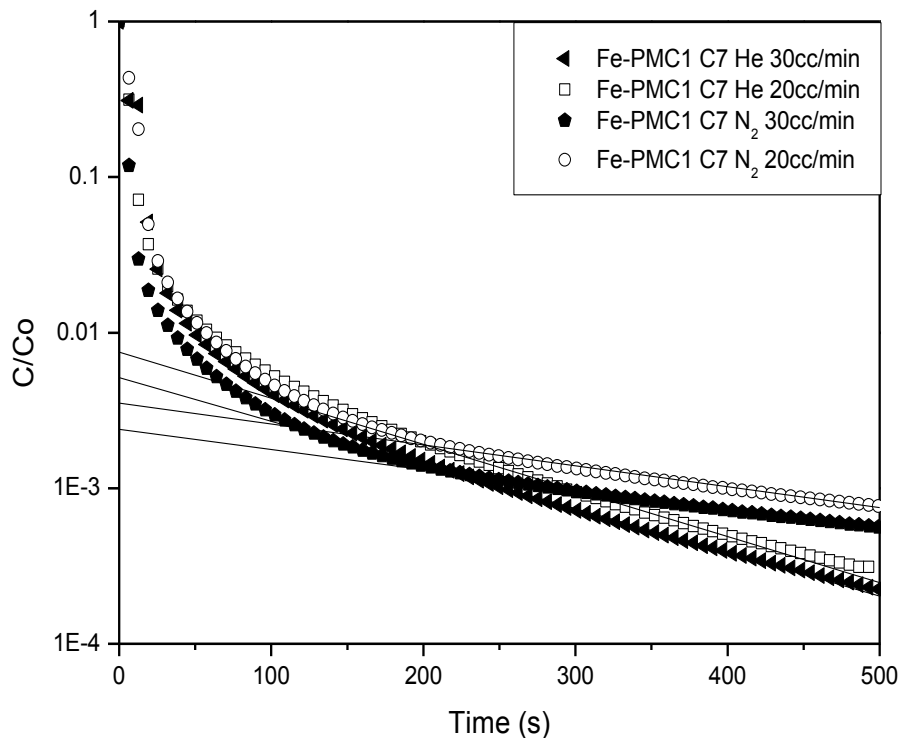


Figure 19 - Comparison of experimental ZLC response curves of Fe-PMC1 at  $P_0 = 0.0054$  bar of  $n-C_7$  in two different purge gas (He and N<sub>2</sub>), 270 °C, 20 and 30 cc/min.

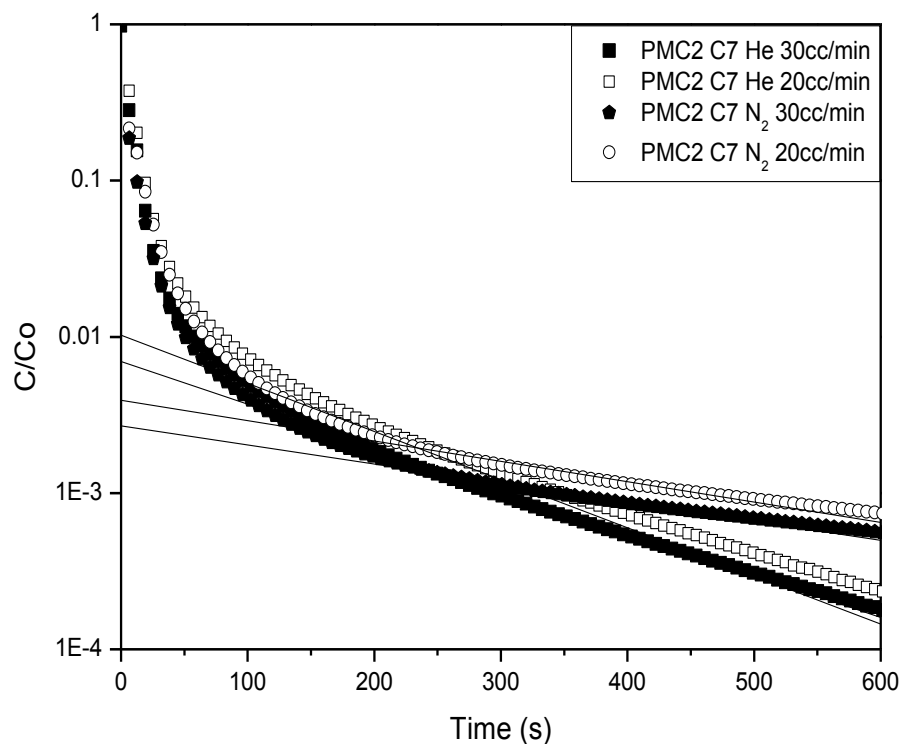


Figure 20 - Comparison of experimental ZLC response curves of PMC2 at  $P_0 = 0.0054$  bar of  $n-C_7$  in two different purge gas (He and N<sub>2</sub>), 270 °C, 20 and 30 cc/min.

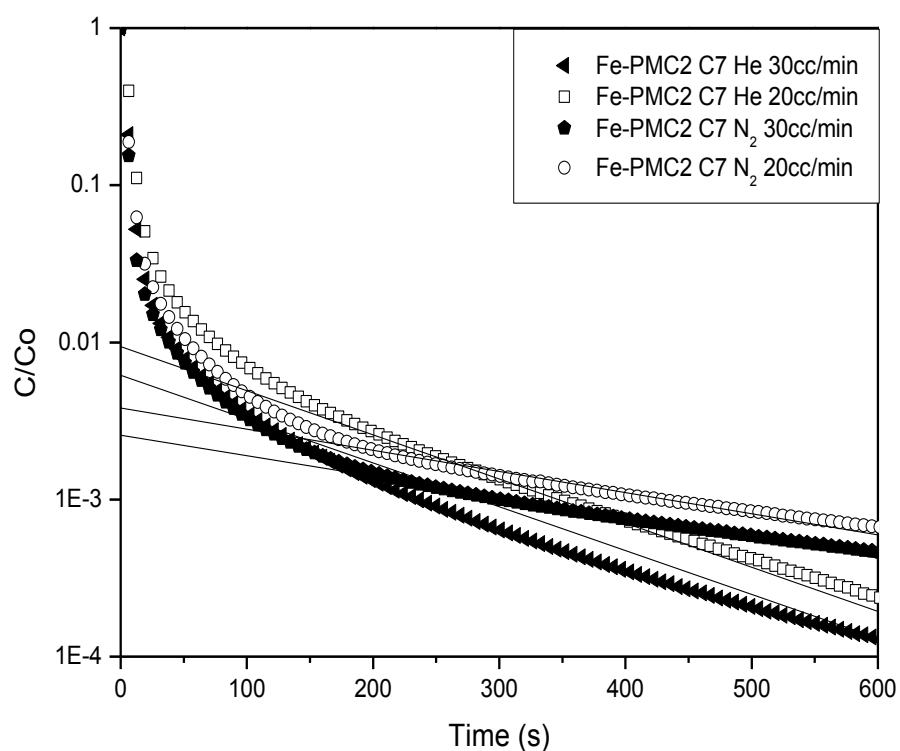


Figure 21 - Comparison of experimental ZLC response curves of Fe-PMC2 at  $P_0 = 0.0054$  bar of  $n-C_7$  in two different purge gas (He and N<sub>2</sub>), 270 °C, 20 and 30 cc/min.

#### 4.4.2 Determination of kinetic control

After defining the predominant diffusion path, it is necessary to confirm that the system is macropore kinetic controlled under the experimental conditions. That is, the desorption rate is controlled by the diffusion of the sorbate out of the particle.

According to Brandani et al. [41], to consider a system under kinetic control, a  $Ft$  plot (flow rate multiplied by time) for each adsorbent measured at a given temperature and adsorbate concentration should diverge at higher purge flow rates [41]. This statement is consistent with the following results and confirmed that the system is macropore kinetic controlled.

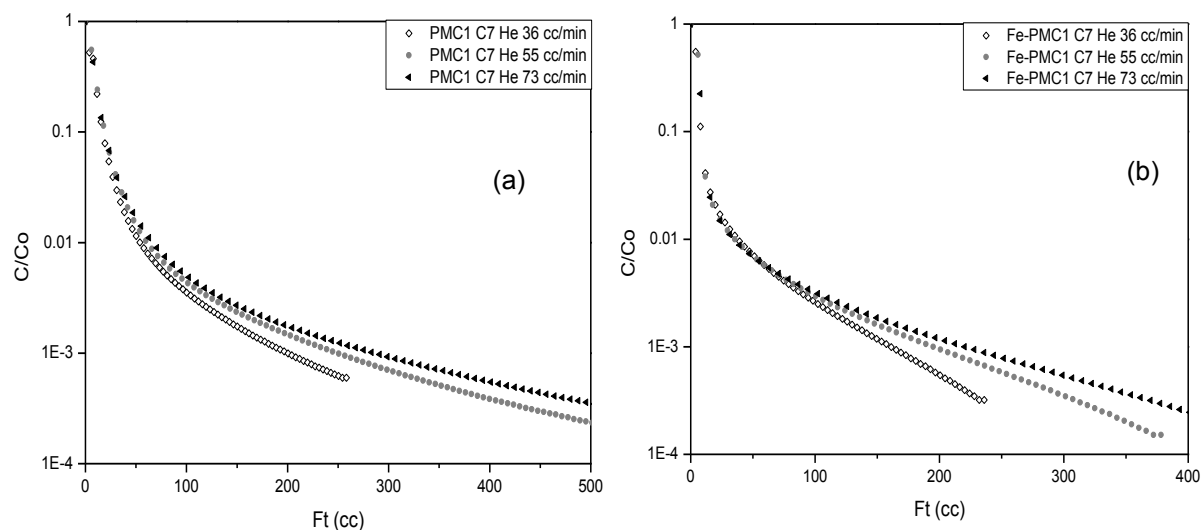


Figure 22 - Plot for *n*-heptane at 270 °C and  $P_0 = 0.0054$  bar in the  $Ft$  form (a) PMC1 (b) Fe-PMC1.

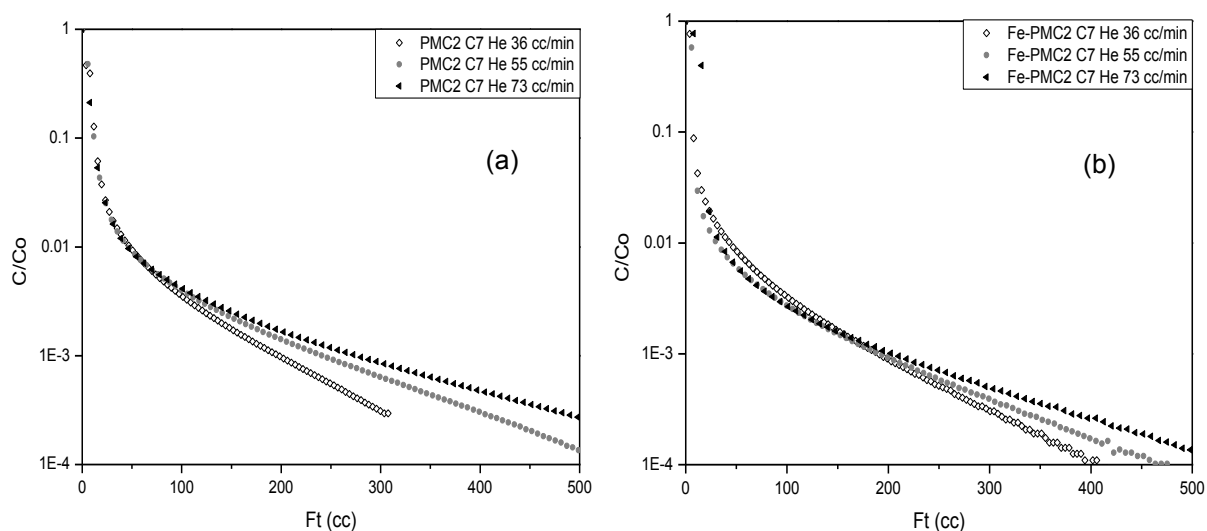


Figure 23 - Plot for *n*-heptane at 270 °C and  $P_0 = 0.0054$  bar in the  $Ft$  form (a) PMC2 (b) Fe-PMC2.

Another other way to confirm if the system is under kinetic control besides the  $Ft$  plot is the evaluation of the  $L$  parameter. If  $L < 1$ , the system is under equilibrium control but if  $L > 5$ , the system is kinetic controlled [34].

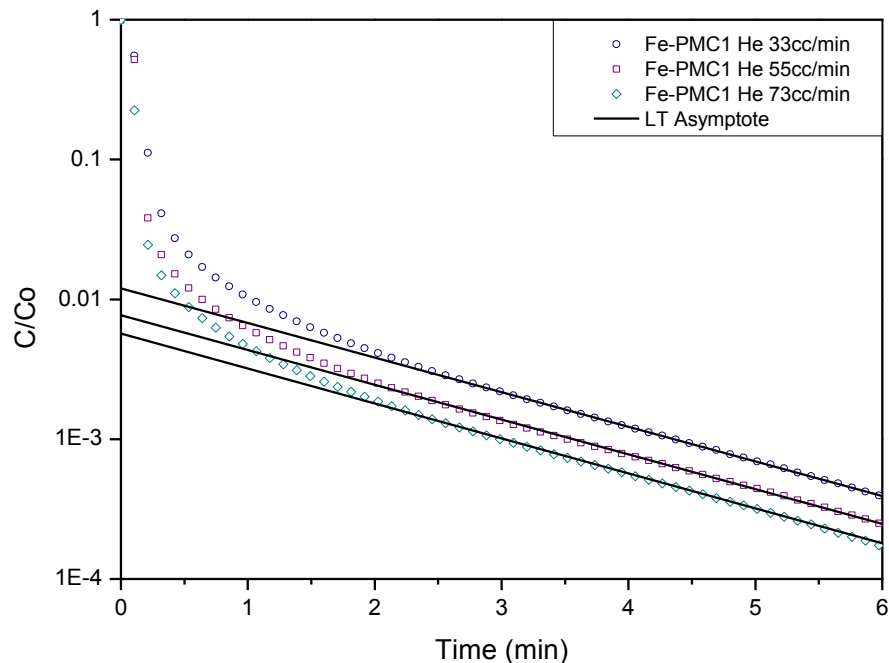


Figure 24- Plot of desorption curves for Fe-PMC1 at 270 °C and  $P_0 = 0.0054$  bar of  $n-C_7$ .

To obtain the  $L$  values, the LT analysis was applied and the results are presented in Table 10. When using the LT analysis in the limit of a very high purge flow rate,  $L \rightarrow \infty$  and  $\beta_1 \rightarrow \pi$ , as presented in Figure 25.

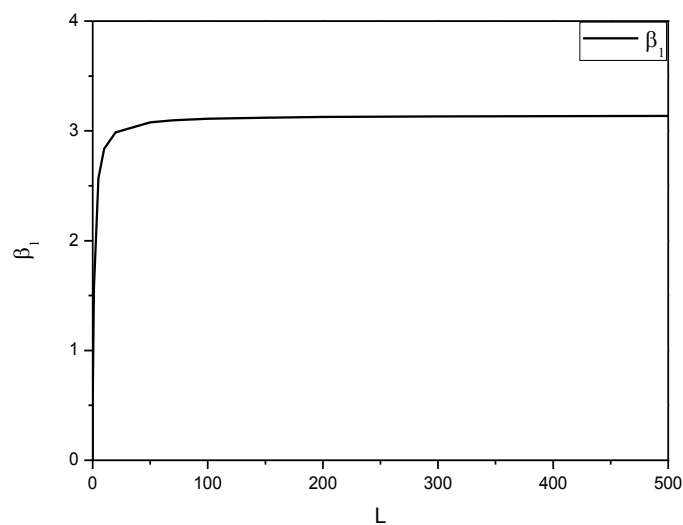


Figure 25 - Variation of  $\beta_1$  with  $L$  according to equation 10.

Thus, equation (12) is reduced to:

$$\frac{c}{c_o} = \frac{2}{L} \exp\left(-\frac{\pi^2 D_p^e t}{R_p^2}\right) \quad (30)$$

Where  $L$  and  $D_p^e/R_p^2$  could be determined directly from the intercept and the slope of a semilogarithmic plot of  $c/c_o$  vs  $t$ . The short time (ST) analysis [34] was not applied in this work due to some limitations on the data acquisition software after switching the valves to an inert purge flow thus compromising the diffusivity results.

Despite the evaluation of the  $L$  parameter and the Ft plot, it is also necessary to check the consistency between the parameter  $L$  and the flow rate [28]. From Equation (11), at a given temperature,  $L$  should be proportional to the purge flow rate with the ratios being shown in Table 10.

Table 10 - Variation of L with flow rate for Fe-PMC1 at different temperatures ( $P_o = 0.0054$  bar of  $n$ - $C_7$ ).

Temperature (°C)	$F$ (cc min <sup>-1</sup> )	$L$	$L^*$ ratio	$F^*$ ratio
210	36	214.45	1.00	
	55	298.55	1.39	1.51
	73	394.77	1.84	2.00
240	36	163.55	1.00	
	55	243.02	1.49	1.51
	73	320.93	1.96	2.00
270	36	173.42	1.00	
	55	250.19	1.44	1.51
	73	341.45	1.97	2.00

\*Relative to values at 36 cc min<sup>-1</sup>  
Source: This research.

It can be observed very good consistency between the ratios of  $L$  and the inert purge flow. However, for Fe-PMC1 at 210 °C a little difference is verified. One can attribute such difference on the choice of the experimental baseline or on the detector limitation when it is operating with high purge flow rates.



### 4.4.3 Evaluation of heat effects

Heat effects can be minimized using high flow rate (high  $L$  values). However, this assumption may not be valid for strongly adsorbed species in large particles under conditions of macropore diffusion control [40, 63, 64].

To verify if the desorption curves of this work were influenced only by mass transfer resistances without heat effects, some considerations were done according to Brandani et al. [40] which neglected the heat effects by fulfilling the following condition:

$$\frac{\alpha\delta}{\gamma} = \left( \frac{|\Delta H_{ads}|}{RT_o} \right)^2 \frac{c_o FR}{haV_s} < 1 \quad (31)$$

with  $\alpha$ ,  $\delta$  and  $\gamma$  being given by the following equations:

$$\alpha = \frac{|\Delta H_{ads}| K c_o}{C_s T_o} \quad (32)$$

$$\delta = \frac{|\Delta H_{ads}|}{RT_o} \quad (33)$$

$$\gamma = \frac{ha KV_s}{C_s F} \quad (34)$$

where  $\Delta H_{ads}$  is the heat of adsorption;  $C_s$  is the volumetric heat capacity of adsorbent particle;  $T_o$  is the ZLC working temperature;  $h$  is the heat transfer coefficient ( $= \varphi/R_p$  for  $Nu = 2$ );  $\varphi$  is the thermal conductivity of carrier gas and  $a$  is the external area/volume for a spherical particle ( $= 3/R_p$ ).

Table 11 summarized the approximate estimates of equation (31) for PMC1 and Fe-PMC1. Unfortunately, adsorption equilibrium experiments for the samples were not carried out, thus not providing heats of adsorption from the Van't Hoff temperature dependence.

Despite that, it was considered that the analyzes of heat effects were in the extreme case in which the hydrocarbons are strongly adsorbed likewise the

results from Díaz et al. [65] which has obtained high values of  $\Delta H_{ads}$  for *n*-heptane and *n*-octane in mesoporous activated carbon using the inverse gas chromatography (IGC) technique under temperature conditions similar to this work.

Table 11 - Significance of heat effects in ZLC experiments.

System	Sample Mass (g)	$V_s$ (cm <sup>3</sup> ) <sup>a</sup>	$R_p$ (cm)	$c_o$ (mol cm <sup>-3</sup> )	$F$ (cm <sup>3</sup> s <sup>-1</sup> )	$-\Delta H_{ads}$ (kcal mol <sup>-1</sup> ) <sup>b</sup>	$\alpha\delta/\gamma$ <sup>c</sup>
<i>n</i> -C <sub>7</sub> -PMC1 210 °C He Carrier	0.0015	0.003	0.025	2.53E-07	0.55	15.83	0.012
					0.92		0.021
					1.22		0.027
<i>n</i> -C <sub>7</sub> -Fe-PMC1 210 °C He Carrier	0.0016	0.001	0.0176	2.34E-07	0.55	15.83	0.020
					0.92		0.033
					1.22		0.044
<i>n</i> -C <sub>8</sub> -PMC1 210 °C He Carrier	0.005	0.008	0.025	2.53E-07	0.55	18.53	0.005
					0.92		0.008
					1.22		0.011
<i>n</i> -C <sub>8</sub> -Fe-PMC1 210 °C He Carrier	0.0042	0.002	0.0176	2.34E-07	0.55	18.53	0.010
					0.92		0.017
					1.22		0.023

<sup>a</sup> -  $V_s = m_{ads}(V_{sv} + V_{pore})$  where  $m_{ads}$  is the sample mass in grams; <sup>b</sup> -  $\Delta H_{ads}$  from literature [65]; <sup>c</sup> -  $\alpha\delta/\gamma$  from literature [66].

Source: This research.

Therefore, even considering the same heat of adsorption for different samples (PMC1 and Fe-PMC1); the criterion  $\alpha\delta/\gamma < 1$  is justified, thus being possible to neglect heat effects on the studied samples.

#### 4.4.4 Determination of the saturation time

After investigating the controlling diffusion mechanism of the desorption process, the appropriated saturation time in which the samples reach the equilibrium

was determined. The importance of the saturation time is to distinguish between diffusion controlled and surface controlled systems [34, 67].

If the system is surface resistance controlled, the dimensionless desorption curves are unaffected by the partial loading. In contrast, in a diffusion controlled system, a partial saturation will provide a dimensionless desorption curves that lie below the response curves for a fully equilibrated sample but with the same asymptotic slope [67]. That is, the partial saturation will provide the largest errors in the intercept and therefore the  $L$  values, thus providing underestimated  $K$  values. Although, the partial saturation, for high  $L$  values, provides errors in the macropore diffusivities that are less than 1% [34].

Some important aspects must be considered to obtain the most appropriated saturation time. Brandani and Ruthven [34] proposed that the saturation time has to be at least equal to  $0.416 R_p^2/D_p^e$ . From this proposal and taking into account that the diffusivity is temperature dependent [25], it is necessary to evaluate the saturation time at the lowest experimental temperature, otherwise it will be underestimated. To verify the correct saturation time, a set of ZLC experiments were performed varying the equilibration time and the results were compared with the condition proposed above.

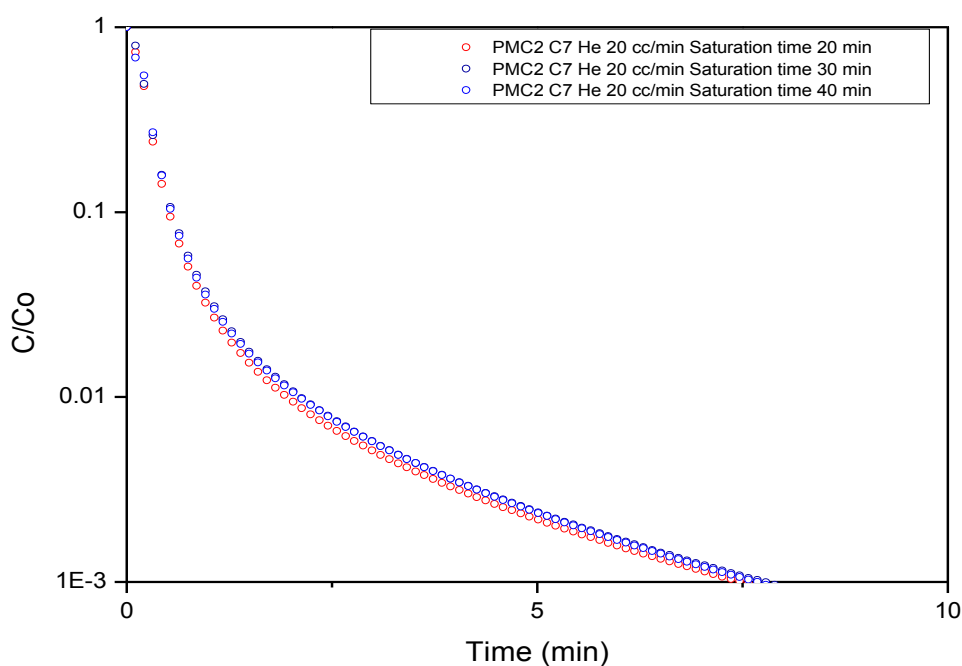


Figure 26 - Influence of the saturation time in experimental ZLC desorption curves for PMC2 at  $P_o = 0.0054$  bar of  $n$ -C<sub>7</sub> with He purge gas, 210 °C, 20 cc/min.

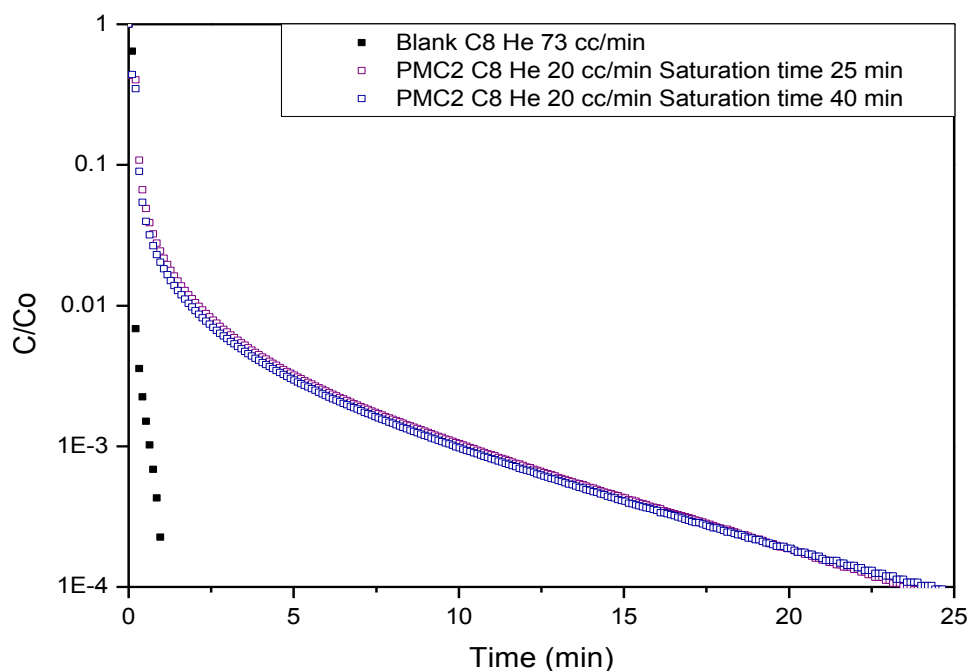


Figure 27 - Influence of the saturation time in experimental ZLC desorption curves for PMC2 at  $P_o = 0.0054$  bar of  $n$ -C<sub>8</sub> with He purge gas, 240 °C, 20 cc/min.

It was considered that all adsorbents in this work have the same saturation time for each adsorbate, 30 min for  $n$ -heptane and 35 min for  $n$ -octane. The increase in saturation time for  $n$ -octane was due to the amount of adsorbent packed inside the ZLC column, however such condition did not influence any diffusion measurement as can be seen in further sections.

From Figure 26 and Figure 27 and the results of Table 12, one may see that the saturation time was experimentally correct.

Table 12 - Determination of the saturation time for PMC2.

Hydrocarbon	Temperature (°C)	$D_p^e/R_p^2$ (s <sup>-1</sup> )	Saturation time (min)
$n$ -heptane	210	5.18E-04	13.4
	240	6.17E-04	11.2
	270	8.39E-04	8.3
$n$ -octane	210	2.02E-04	34.4
	240	2.46E-04	28.2
	270	2.68E-04	25.9

Source: This research.

Another aspect that can be evaluated is to check if the dead volume influence the desorption process. This may be verified for the blank runs (without adsorbent) in Figure 27, of which the response curves are clearly faster, thus indicating no influence on the results of the adsorbent desorption curves.

#### 4.4.5 Influence of the flow rate in the kinetics of adsorption

Under conditions of kinetic control the reciprocal diffusional time constant determined from the asymptotic slope of the plot  $c/c_0$  vs  $t$  should be independent of flow rate [38, 67] because as established on a previous section, at higher  $L$  values,  $\beta_1 \rightarrow \pi$ .

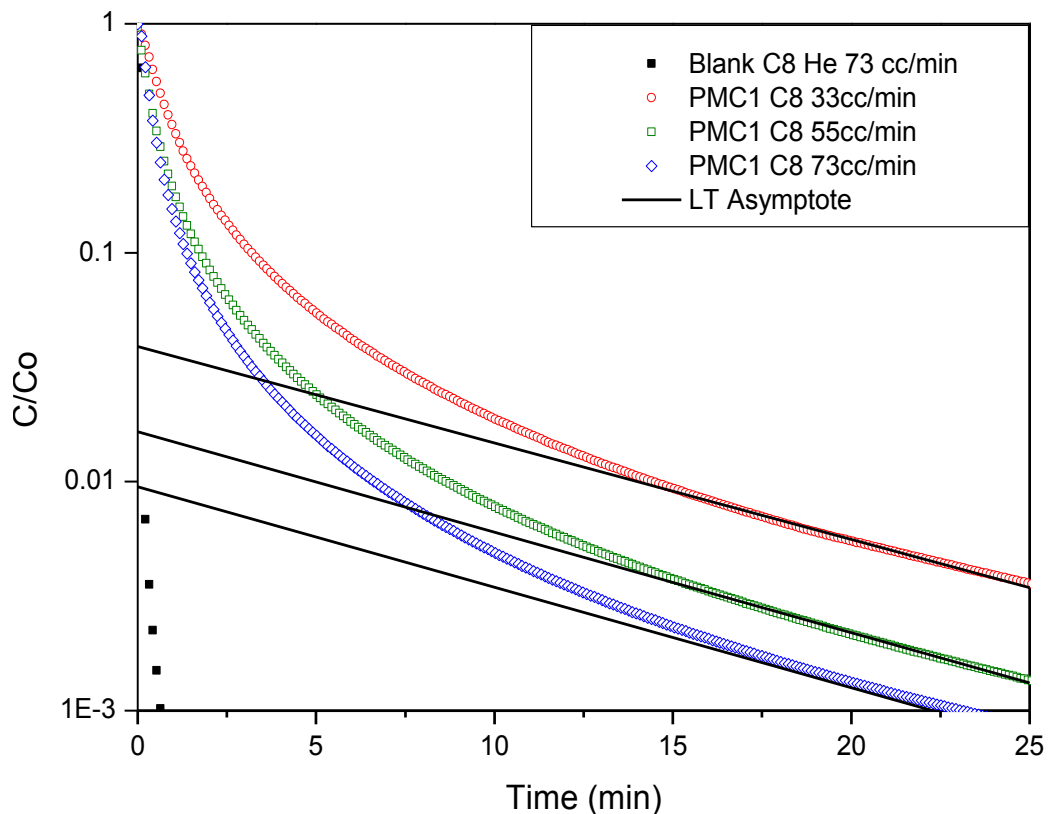


Figure 28 - Influence of the flow rate on desorption plot.

From Figure 28, this consistency is observed and the results are presented below (Table 13) for the adsorbent PMC1. This statement is in accordance with all samples used in this work.

Table 13 - Influence of flow rate in kinetic data for PMC1 at 210 °C and  $P_0 = 0.0054$  bar of *n*-octane.

Flow rate (cc min <sup>-1</sup> )	$L$	$\beta_1^2$	$D_p^e/R_p^2$ (s <sup>-1</sup> )	$D_p^e$ (cm <sup>2</sup> s <sup>-1</sup> ) $\times 10^8$
36	45.3	9.4	1.74E-04	10.9
55	118.2	9.7	1.68E-04	10.5
73	214.2	9.8	1.66E-04	10.4

Source: This research.

#### 4.4.6 Influence of the temperature in the kinetics of adsorption

The macropore diffusivity of binary gas mixtures is dependent on the temperature and is independent on concentration [25]. In order to evaluate the influence of the temperature in the asymptotic slope from the LT analysis, Ruthven and Xu [30] plotted different desorption response curves with the same flow rate under different temperatures.

The authors verified that the macropore reciprocal diffusional time constant increases with temperature. As a matter of fact, this trend was also observed in the following ZLC results (Figure 29) for PMC2 and their corresponding macropore diffusion data is presented in Table 14. The same trend occurred for all adsorbents and can be observed in further sections.

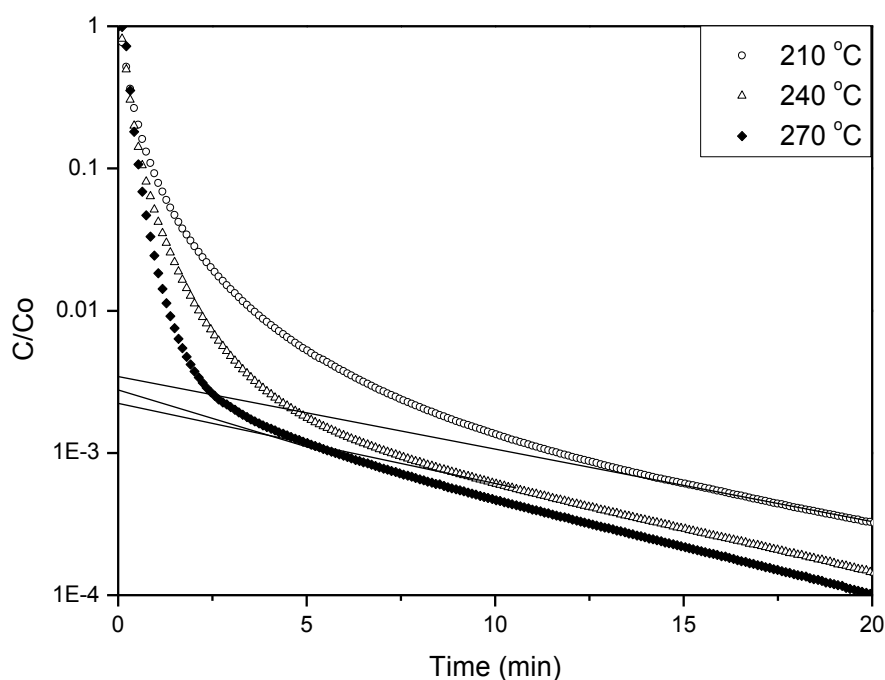


Figure 29 - ZLC Desorption Curves for *n*-C<sub>8</sub> in PMC2 showing the effects of temperature. Purge gas He at 73 cc/min.

Table 14 - Macropore diffusion data of  $n\text{-C}_8$  in PMC2 at different temperatures.

Temperature (°C)	$D_p^e/R_p^2$ ( $\text{s}^{-1}$ ) $\times 10^4$	$D_p^e$ ( $\text{cm}^2 \text{s}^{-1}$ ) $\times 10^8$
210	2.02	10.2
240	2.46	12.4
270	2.68	13.6

Source: This research.

#### 4.4.7 Influence of the adsorbent mass in the kinetic data

The basic modelling assumption for the ZLC method is to consider the column sufficiently short so that the inter-particle transport barriers are reduced and the system behaves like a perfectly mixed cell. This can be experimentally checked by changing the amount of adsorbent until the diffusion measurements were independent of the adsorbent amount packed [39].

Brandani et al [38] discussed the impact of sample amount on diffusion measurements and observed that desorption curves slowed as the amount of sample increases due to the influence of convective effects, such as external hold-up or heat effects.

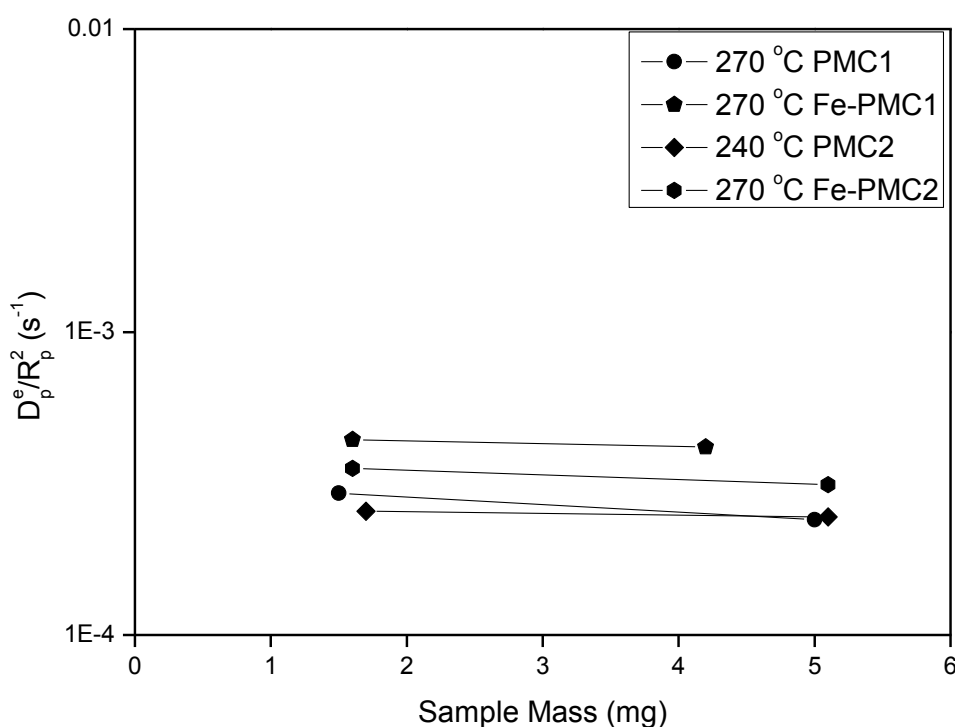


Figure 30 - Effect of sample quantity in the macropore reciprocal diffusional time constant.

In an effort to verify such influence in our ZLC system (Figure 30), sample mass was increased for PMC1, PMC2, Fe-PMC1 and Fe-PMC2 and the macropore reciprocal diffusional time constants were evaluated.

Table 15 - Influence of the sample mass in  $n$ -C<sub>8</sub> diffusion measurements for PMC1 and Fe-PMC1 at 270 °C and P<sub>o</sub> = 0.0054 bar.

Adsorbent	Sample mass (mg)	$D_p^e/R_p^2$ (s <sup>-1</sup> ) × 10 <sup>4</sup>	$D_p^e$ (cm <sup>2</sup> s <sup>-1</sup> ) × 10 <sup>8</sup>
PMC1	1.5	2.93	18.4
	5	2.4	15.0
Fe-PMC1	1.6	4.42	13.7
	4.2	4.17	12.9

Source: This research.

From the obtained results (Table 15), one may infer that ZLC system behaves like a perfectly mixed cell for all adsorbents and the macropore diffusivity practically remains constant over the mass amount (1.5–5.1 mg) applied in the tests. Therefore, the ZLC modelling assumptions are fulfilled experimentally being possible to neglect heat effects and external mass transfer resistance on the studied samples.

#### 4.4.8 Influence of concentration in the kinetic data

In order to observe the influence of the concentration on the obtained kinetics data, a set of ZLC experiments were run with different concentrations only on PMC2.

The experiments with different concentrations were carried out using  $n$ -heptane, being the ones under the lowest concentration carried out under the same conditions at the *University of Edinburgh* (UoE) due to limitations in our ZLC system. The ZLC apparatus from UoE had a more accurate FID, capable of detecting the hydrocarbons at considerably lower concentrations. Giving such conditions of concentration, it has been assumed that the UoE ZLC system operated under the linear region, nevertheless adsorption equilibrium measurements for all adsorbents are necessary to confirm the linearity [39].

Another critical assumption when modelling the ZLC is that the system is under linear equilibrium. This assumption is however not valid when considering



strongly adsorbed species or when the concentration is purposely increased to improve the detector's signal which may give systems operating under non equilibrium conditions [39]. For this reason, Brandani [39] studied the different aspects in which the concentration may influence the experimental desorption curves, such as the diffusivity, dimensionless Henry constant and  $L$  parameter.

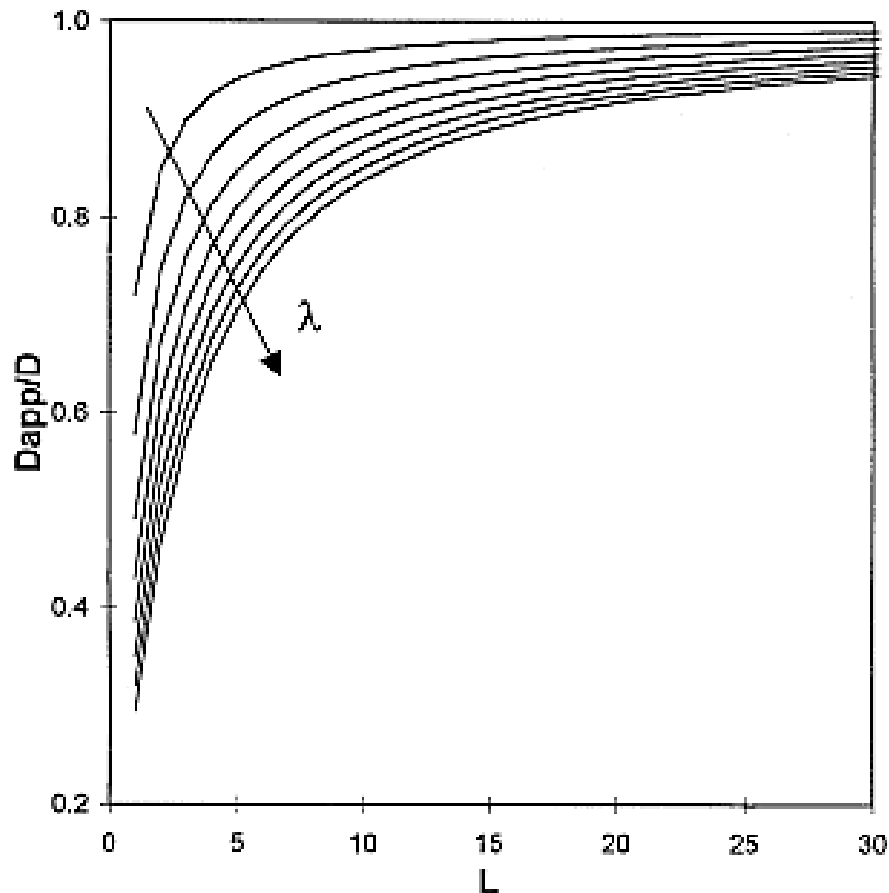


Figure 31 - Effect of nonlinear equilibrium on the apparent diffusivity obtained from the application of the LT asymptote analysis.  $\lambda = 0.1, 0.2, 0.3, 0.4, 0.5, 0.6, 0.7, 0.8$  [39].

The influence on the apparent diffusivity ( $D_{app}$ ), which may be the particle effective diffusivity or the intracrystalline diffusivity, when the system is under nonlinear conditions is shown in Figure 31. One may see that no significant difference in the apparent diffusivity is observed at higher  $L$  values. That is, under nonlinear conditions the concentration falls to values so low that the model becomes linear providing a reciprocal diffusional time constant (slope of LT asymptote) similar to the linear model [39].

The derived macropore diffusivities obtained from the asymptotic slope of Figure 32 and Figure 33 show that even with large increase steps in concentration,

the particle effective diffusivity values are in the same order magnitude with a small difference between them (Table 16). Thus, the system may have some evidences that it is under nonlinear conditions because other effects such as external hold-up and heat effects have been previously discarded.

Table 16 - Macropore diffusivity of  $n\text{-C}_7$  in PMC2 at a temperature of 270 °C in different concentrations.

Concentration (ppm)	$D_p^e/R_p^2$ (s <sup>-1</sup> )	$D_p^e$ (cm <sup>2</sup> s <sup>-1</sup> ) × 10 <sup>8</sup>
25	1.12E-03	56.7
5370	8.39E-04	42.5

Source: This research.

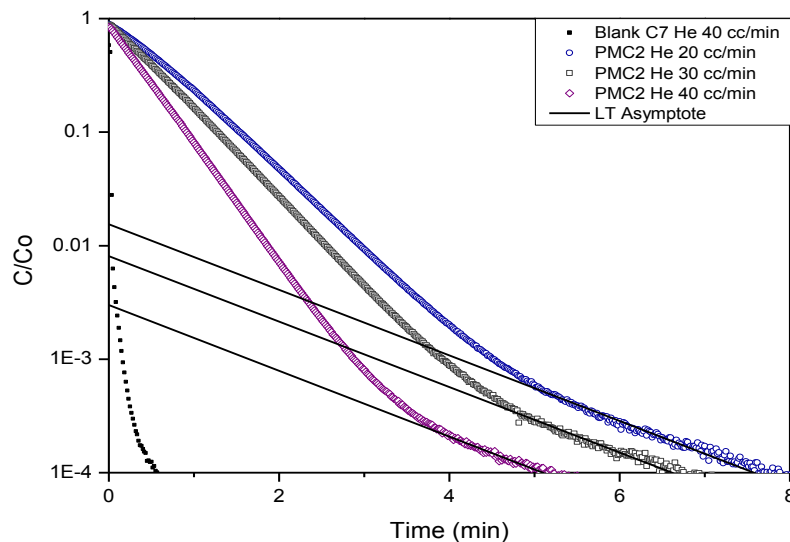


Figure 32 - Desorption response curves of  $n\text{-C}_7$  in PMC2 at 270 °C and  $c_0 = 25$  ppm.

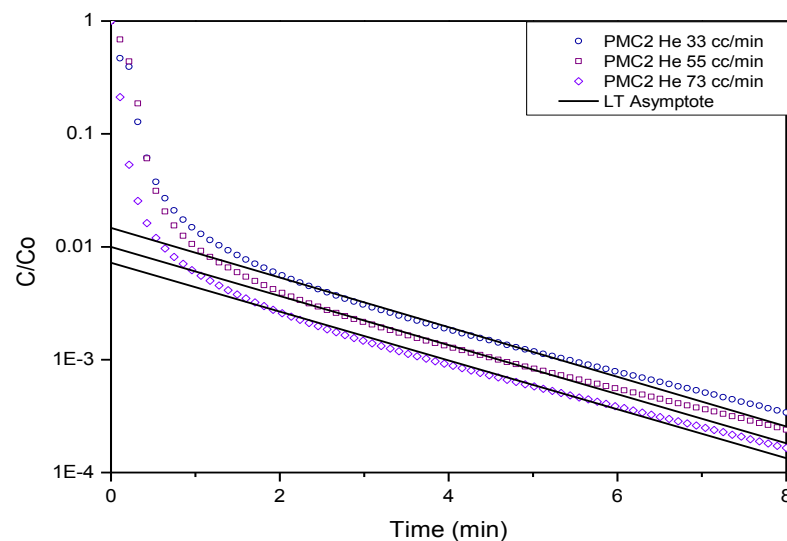


Figure 33 - Desorption response curves of  $n\text{-C}_7$  in PMC2 at 270 °C and  $c_0 = 5370$  ppm.

#### 4.4.9 Diffusion of linear paraffins in activated carbons supports and Fe-based catalysts supported on AC

To understand the influence of different hydrocarbon chains in diffusion measurements, Cavalcante and Ruthven [32] observed the following trend for diffusion measurements of branched and cyclic alkanes in silicalite (fastest to slowest): linear > single-branched > double-branched (ternary-C) > cyclic > double-branched (quaternary-C) alkanes.

Despite the lack of reports evaluating the diffusion measurements of linear paraffins on activated carbons by the ZLC technique, studies using bi-porous adsorbents materials (mostly zeolites) along with the trend observed above have supported the following results [30, 32, 36, 43, 68].

In order to determine the diffusion behavior of each adsorbate, the following results were obtained according to the conditions presented in Table 4 which are similar to those used for Fischer-Tropsch reactions.

##### 4.4.9.1 *n*-heptane and *n*-octane

The measurements of *n*-C<sub>7</sub> and *n*-C<sub>8</sub> diffusion in all adsorbents are summarized in Table 17. As expected, the macropore diffusivity increased with temperature for all adsorbents and the AC supports presented lower diffusion resistances in comparison with the iron catalysts. This behavior might be associated to the relatively larger pore volumes and sizes of the supports, which posed less transport resistance to the adsorbed molecules.

Besides the comparison of the diffusivity values between the adsorbents, the following diffusion results also helped to verify if the system reached full equilibrium before starting the desorption process. Brandani and Ruthven [34], proposed that the saturation time has to be at least equal to  $0.416 R_p^2 / D_p^e$ . Therefore, after applying this condition, the calculated saturation time for the adsorbents were in accordance with the ones obtained experimentally and thus giving the correct system parameters.

Table 17 - Diffusion measurements of  $n\text{-C}_7$  and  $n\text{-C}_8$  on the AC supports and on Fe-based catalysts supported on AC.

Adsorbent	Temperature (°C)	<i>n</i> -heptane	<i>n</i> -octane
		$D_p^e$ (cm <sup>2</sup> s <sup>-1</sup> ) × 10 <sup>8</sup>	$D_p^e$ (cm <sup>2</sup> s <sup>-1</sup> ) × 10 <sup>8</sup>
PMC1	210	25.8	10.6
	240	34.1	14.0
	270	46.0	15.0
Fe-PMC1	210	18.9	9.1
	240	22.8	11.2
	270	30.0	12.9
PMC2	210	26.2	10.2
	240	31.4	12.4
	270	42.5	13.6
Fe-PMC2	210	21.1	6.1
	240	26.8	10.7
	270	30.0	12.2

Source: This research.

From the results of Table 17, it is evident that the macropore diffusivity decreased with increasing paraffin chains ( $n\text{-octane} < n\text{-heptane}$ ), which was the same behavior reported for silicalite [32].

Despite the absence of data regarding diffusion in carbon-based materials using the ZLC, the macropore diffusivities obtained for  $n\text{-heptane}$  and  $n\text{-octane}$  are correctly evaluated because all the ZLC assumptions were fulfilled.

#### 4.4.9.2 *n*-dodecane

Several experiments with  $n\text{-C}_{12}$  in Fe-PMC2 were carried out, however, the ZLC system was not able to provide good experimental signal for a low pressure condition of  $n\text{-dodecane}$ . For that reason, the ZLC experimental curves were under the experimental error of the detector which provided results without any apparent physical meaning (Figure 34).

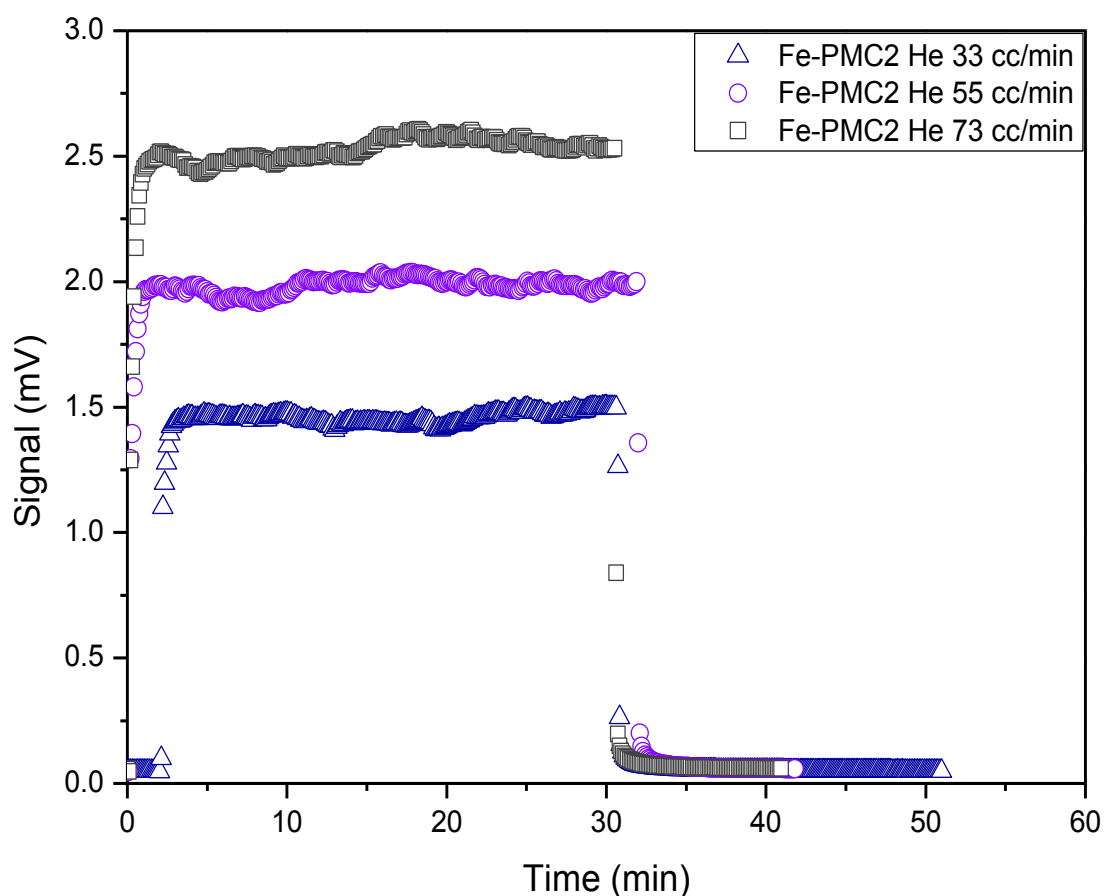


Figure 34 - ZLC experimental signal of *n*-dodecane at 210 °C.

#### 4.4.10 Analysis of the diffusion process

Keil [27] distinguished the diffusion within the pores as a combination of three different mechanisms: molecular diffusion, Knudsen diffusion and surface diffusion. However, at temperatures far above the boiling point of the physical adsorbed species, the contribution of surface diffusion is little [24]. Surface diffusion contribution is not considered because the experimental temperature is much higher than the boiling point of *n*-heptane and *n*-octane.

To understand which diffusion mechanism is influencing the macropore diffusivity values obtained from the ZLC, a detailed analysis of the data is presented. From the macropore diffusion model following the ZLC assumptions {equation (28)}, one may see that the effective pore diffusivity is a function of the overall macropore diffusivity ( $D_{macro}$ ). According to Hu et al. [43],  $D_{macro}$  is defined by the following equation:

$$\frac{1}{D_{macro}} = \frac{1}{D_m} + \frac{1}{D_K} \quad (35)$$

where  $D_m$  is the molecular and  $D_K$  is the Knudsen diffusivities. In which from Bird et al. [25]:

$$D_m = \frac{3}{16} \frac{\sqrt{2\pi RT_o \left( \frac{1}{M_1} + \frac{1}{M_2} \right)}}{\frac{P}{kT_o} \sigma_{12}^2 \Omega_{D,12}} \quad (36)$$

and from Ruthven [24]:

$$D_K = 9700 \frac{D_{pore}}{2} \left( \frac{T_o}{M} \right)^{1/2} \quad (37)$$

where  $k$  is the Boltzmann constant;  $M$  is the molecular weight of the diffusing species;  $P$  is the total pressure;  $\sigma_{12}$  is a characteristic length parameter of the binary pair and  $\Omega_{D,12}$  represents the collision integral. The Knudsen diffusivity was calculated using the pore diameter obtained from the adsorbent textural characterization.

In Table 18 the diffusion contributions are summarized. From the results, one may infer that both molecular and Knudsen diffusivity are not predominant in the effective pore diffusivity. This is true because the pore diameter of the adsorbents is much larger than hydrocarbons molecular length in the case of Knudsen diffusivity and in the case of molecular diffusivity, the system is working at atmospheric pressure ( $\sim 1$  atm) reducing the molecular diffusivity contribution.

Therefore, it may be said that the main contribution in the macropore diffusivity comes from the dimensionless Henry constant {denominator of equation (27)} even though this parameter not being evaluated in this work. A similar conclusion was obtained in the literature [43].

Table 18 - Summary of the diffusion contributions in the effective pore diffusivity.

Adsorbent	Adsorbate	Temperature (°C)	$D_m$ (cm <sup>2</sup> s <sup>-1</sup> )	$D_K$ (cm <sup>2</sup> s <sup>-1</sup> )	$\varepsilon_p D_{macro}$ (cm <sup>2</sup> s <sup>-1</sup> )	$D_p^e$ (cm <sup>2</sup> s <sup>-1</sup> )
PMC1	<i>n</i> -heptane	210	6.12E-01	2.77E-03	2.09E-03	2.58E-07
		240	6.77E-01	2.85E-03	2.16E-03	3.41E-07
		270	7.45E-01	2.94E-03	2.22E-03	4.60E-07
	<i>n</i> -octane	210	5.63E-01	2.59E-03	1.96E-03	1.06E-07
		240	6.23E-01	2.67E-03	2.02E-03	1.40E-07
		270	6.85E-01	2.75E-03	2.08E-03	1.50E-07
PMC2	<i>n</i> -heptane	210	6.12E-01	2.98E-03	2.31E-03	2.622E-07
		240	6.77E-01	3.07E-03	2.39E-03	3.124E-07
		270	7.45E-01	3.16E-03	2.46E-03	4.247E-07
	<i>n</i> -octane	210	5.63E-01	2.79E-03	2.17E-03	1.023E-07
		240	6.23E-01	2.88E-03	2.23E-03	1.24E-07
		270	6.85E-01	2.96E-03	2.30E-03	1.357E-07
Fe-PMC1	<i>n</i> -heptane	210	6.12E-01	2.56E-03	1.30E-03	1.885E-07
		240	6.77E-01	2.63E-03	1.34E-03	2.284E-07
		270	7.45E-01	2.71E-03	1.38E-03	2.999E-07
	<i>n</i> -octane	210	5.63E-01	2.39E-03	1.22E-03	9.129E-08
		240	6.23E-01	2.47E-03	1.25E-03	1.117E-07
		270	6.85E-01	2.54E-03	1.29E-03	1.29E-07
Fe-PMC2	<i>n</i> -heptane	210	6.12E-01	1.81E-03	5.96E-04	2.114E-07
		240	6.77E-01	1.87E-03	6.14E-04	2.681E-07
		270	7.45E-01	1.92E-03	6.32E-04	2.996E-07
	<i>n</i> -octane	210	5.63E-01	1.70E-03	5.58E-04	6.101E-08
		240	6.23E-01	1.75E-03	5.75E-04	1.069E-07
		270	6.85E-01	1.80E-03	5.92E-04	1.22E-07

Source: This research.

## 5 SUMMARY AND CONCLUSIONS

### ***About the use of the ZLC technique to obtain diffusion measurements***

As verified in Chapter 4, the diffusion measurements were proved to be kinetically controlled and to verify if the adsorbents are well analyzed, blank runs were carried out in order to verify if the system under the experimental conditions have the capacity to adsorb the linear paraffins. It is clear from the presented results that the desorption blank runs were under the response curves thus indicating that the dead volume of the system does not influence the diffusion measurements.

According to Brandani [39], in order to avoid any arbitrary diffusivity value, the experiments with the adsorbents under the same temperature have to be carried out in different flows and their reciprocal diffusional time constant should be the same at higher  $L$  values. This statement was correctly verified in all samples. In addition, the dimensionless parameter  $L$  was also important because it evaluated that the system was under macropore kinetic control.

Also, it can be pointed out that this study evaluated successfully the different parameters that may influence the diffusion measurements by the ZLC technique, indicating that all the experiments were carried out fulfilling all assumptions when modelling a ZLC system.

### ***About the diffusion measurements of linear paraffins in the studied adsorbents***

The trimodal pore structure verified by nitrogen isotherms along with desorption experiments of linear paraffins carried by different purge inert gases indicated that the macropore diffusion is controlling the desorption process. As a consequence, the effective pore diffusivity is a combination of different diffusivities, such as the molecular and Knudsen [27]. However, it was demonstrated that the main contribution might be due to the dimensionless Henry law constant.



## REFERENCES

1. Liu, Z.-P. and P. Hu, *A New Insight into Fischer–Tropsch Synthesis*. Journal of the American Chemical Society, 2002. **124**(39): p. 11568-11569.
2. Ma, W., E.L. Kugler, and D.B. Dadyburjor, *Effect of Properties of Various Activated-Carbon Supports and Supported Fe–Mo–Cu–K Catalysts on Metal Precursor Distribution, Metal Reduction, and Fischer–Tropsch Synthesis*. Energy & Fuels, 2010. **24**(8): p. 4099-4110.
3. Ribeiro, M.C., et al., *Fischer–Tropsch Synthesis: Influence of Mn on the Carburization Rates and Activities of Fe-Based Catalysts by TPR-EXAFS/XANES and Catalyst Testing*. The Journal of Physical Chemistry C, 2011. **115**(11): p. 4783-4792.
4. Dry, M.E., *The Fischer–Tropsch process: 1950–2000*. Catalysis Today, 2002. **71**(3–4): p. 227-241.
5. Newsome, D.S., *The water-gas shift reaction*. Catalysis Reviews Science and Engineering, 1980. **21**(2): p. 275-318.
6. Dry, M.E., *Fischer–Tropsch reactions and the environment*. Applied Catalysis A: General, 1999. **189**(2): p. 185-190.
7. Van Der Laan, G.P. and A.A.C.M. Beenackers, *Kinetics and Selectivity of the Fischer–Tropsch Synthesis: A Literature Review*. Catalysis Reviews, 1999. **41**(3-4): p. 255-318.
8. Zhang, Q., J. Kang, and Y. Wang, *Development of Novel Catalysts for Fischer–Tropsch Synthesis: Tuning the Product Selectivity*. ChemCatChem, 2010. **2**(9): p. 1030-1058.
9. Bukur, D.B., et al., *Binder/support effects on the activity and selectivity of iron catalysts in the Fischer-Tropsch synthesis*. Industrial & Engineering Chemistry Research, 1990. **29**(8): p. 1588-1599.
10. Khodakov, A.Y., et al., *Pore Size Effects in Fischer Tropsch Synthesis over Cobalt-Supported Mesoporous Silicas*. Journal of Catalysis, 2002. **206**(2): p. 230-241.
11. Abbaslou, R.M.M., J. Soltan, and A.K. Dalai, *Effects of nanotubes pore size on the catalytic performances of iron catalysts supported on carbon nanotubes for Fischer–Tropsch synthesis*. Applied Catalysis A: General, 2010. **379**(1–2): p. 129-134.
12. Ma, W., et al., *Mo–Fe Catalysts Supported on Activated Carbon for Synthesis of Liquid Fuels by the Fischer–Tropsch Process: Effect of Mo Addition on Reducibility, Activity, and Hydrocarbon Selectivity*. Energy & Fuels, 2006. **20**(6): p. 2299-2307.
13. Serp, P., M. Corrias, and P. Kalck, *Carbon nanotubes and nanofibers in catalysis*. Applied Catalysis A: General, 2003. **253**(2): p. 337-358.
14. Lee, J., et al., *Metal-organic framework materials as catalysts*. Chemical Society Reviews, 2009. **38**(5): p. 1450-1459.
15. Karaca, H., et al., *Structure and catalytic performance of Pt-promoted alumina-supported cobalt catalysts under realistic conditions of Fischer–Tropsch synthesis*. Journal of Catalysis, 2011. **277**(1): p. 14-26.
16. de Smit, E., et al., *Local and long range order in promoted iron-based Fischer–Tropsch catalysts: A combined in situ X-ray absorption spectroscopy/wide angle X-ray scattering study*. Journal of Catalysis, 2009. **262**(2): p. 244-256.

17. Borg, Ø., et al., *Fischer–Tropsch synthesis over un-promoted and Re-promoted  $\gamma$ -Al<sub>2</sub>O<sub>3</sub> supported cobalt catalysts with different pore sizes*. *Catalysis Today*, 2009. **142**(1–2): p. 70-77.
18. Hong, J., et al., *Effect of promotion with ruthenium on the structure and catalytic performance of mesoporous silica (smaller and larger pore) supported cobalt Fischer–Tropsch catalysts*. *Catalysis Today*, 2009. **140**(3–4): p. 135-141.
19. Jacobs, G., et al., *Fischer–Tropsch synthesis: support, loading, and promoter effects on the reducibility of cobalt catalysts*. *Applied Catalysis A: General*, 2002. **233**(1–2): p. 263-281.
20. Bell, A.T., *The Impact of Nanoscience on Heterogeneous Catalysis*. *Science*, 2003. **299**(5613): p. 1688-1691.
21. Do, D.D., *Adsorption Analysis: Equilibria and Kinetics*. 1998: Imperial College Press.
22. Marsh, H. and F.R. Reinoso, *Activated Carbon*. 2006: Elsevier Science.
23. Sing, K.S.W., *10 - Adsorption by Active Carbons*, in *Adsorption by Powders and Porous Solids (Second Edition)*, F.R.R.S.W.S.L. Maurin, Editor. 2014, Academic Press: Oxford. p. 321-391.
24. Ruthven, D.M., *Principles of Adsorption and Adsorption Processes*. 1984: Wiley.
25. Bird, R.B., W.E. Stewart, and E.N. Lightfoot, *Transport Phenomena*. 2007: Wiley.
26. Kärger, J., D.M. Ruthven, and D.N. Theodorou, *Diffusion in Nanoporous Materials*. 2012: Wiley.
27. Keil, F.J., *Diffusion and reaction in porous networks*. *Catalysis Today*, 1999. **53**(2): p. 245-258.
28. Eic, M. and D.M. Ruthven, *A New Experimental-Technique for Measurement of Intracrystalline Diffusivity*. *Zeolites*, 1988. **8**(1): p. 40-45.
29. Micke, A., M. Kočirik, and M. Bülow, *Theory of zero length column chromatography with the condition of a well-stirred sorbing zone*. *Microporous Materials*, 1993. **1**(6): p. 373-381.
30. Ruthven, D.M. and Z. Xu, *Diffusion of Oxygen and Nitrogen in 5a Zeolite Crystals and Commercial 5a Pellets*. *Chemical Engineering Science*, 1993. **48**(18): p. 3307-3312.
31. Hufton, J.R., S. Brandani, and D.M. Ruthven, *Measurement of Intracrystalline Diffusion by Zero Length Column Tracer Exchange*, in *Studies in Surface Science and Catalysis*, H.G.K.H.P. J. Weitkamp and W. Hölderich, Editors. 1994, Elsevier. p. 1323-1330.
32. Cavalcante Jr., C.L. and D.M. Ruthven, *Adsorption of Branched and Cyclic Paraffins in Silicalite. 2. Kinetics*. *Industrial & Engineering Chemistry Research*, 1995. **34**(1): p. 185-191.
33. Brandani, S. and D.M. Ruthven, *Analysis of ZLC desorption curves for liquid systems*. *Chemical Engineering Science*, 1995. **50**(13): p. 2055-2059.
34. Brandani, S. and D.M. Ruthven, *Analysis of ZLC desorption curves for gaseous systems*. *Adsorption-Journal of the International Adsorption Society*, 1996. **2**(2): p. 133-143.
35. Brandani, S. and D.M. Ruthven, *Moments analysis of the zero length column method*. *Industrial & Engineering Chemistry Research*, 1996. **35**(1): p. 315-319.

36. Brandani, S., *Analytical solution for ZLC desorption curves with bi-porous adsorbent particles*. Chemical Engineering Science, 1996. **51**(12): p. 3283-3288.
37. Silva, J.C. and A.E. Rodrigues, *Analysis of ZLC technique for diffusivity measurements in bidisperse porous adsorbent pellets*. Gas Separation & Purification, 1996. **10**(4): p. 207-224.
38. Brandani, S., Z. Xu, and D. Ruthven, *Transport diffusion and self-diffusion of benzene in NaX and CaX zeolite crystals studied by ZLC and tracer ZLC methods*. Microporous Materials, 1996. **7**(6): p. 323-331.
39. Brandani, S., *Effects of nonlinear equilibrium on zero length column experiments*. Chemical Engineering Science, 1998. **53**(15): p. 2791-2798.
40. Brandani, S., et al., *Heat Effects in ZLC Experiments*. Adsorption, 1998. **4**(3-4): p. 275-285.
41. Brandani, S., M.A. Jama, and D.M. Ruthven, *ZLC Measurements under non-linear conditions*. Chemical Engineering Science, 2000. **55**(7): p. 1205-1212.
42. Silva, J.A.C., K. Schumann, and A.E. Rodrigues, *Sorption and kinetics of CO<sub>2</sub> and CH<sub>4</sub> in binderless beads of 13X zeolite*. Microporous and Mesoporous Materials, 2012. **158**: p. 219-228.
43. Hu, X.Y., et al., *Diffusion mechanism of CO<sub>2</sub> in 13X zeolite beads*. Adsorption-Journal of the International Adsorption Society, 2014. **20**(1): p. 121-135.
44. Böhringer, B., et al., *Polymer-based Spherical Activated Carbons—From Adsorptive Properties to Filter Performance*. Chemie Ingenieur Technik, 2011. **83**(1-2): p. 53-60.
45. Cruz, M.G.A., et al., *On the structural, textural and morphological features of Fe-based catalysts supported on polystyrene mesoporous carbon for Fischer-Tropsch synthesis*. Applied Catalysis a-General, 2015. **495**: p. 72-83.
46. Cruz, M.G.A., *Síntese e Análise de Catalisadores de Ferro Suportados em Carbono Ativado para Síntese de Fischer-Tropsch*, in Departamento de Engenharia Química 2014, Universidade Federal do Ceará. p. 89.
47. Cruz, M.G.A., *Desenvolvimento de Catalisador de Ferro Suportado em Carbono Ativado a Base de Polímeros para Síntese de Fischer-Tropsch*, 2011, Universidade Federal do Ceará. p. 38.
48. von, B.H., B.D. Böhringer, and J.M. Giebelhausen, *Hochleistungsadsorbentien auf Basis von Aktivkohle mit hoher Mikroporosität*, 2008, Google Patents.
49. Bandoz, T.J. and C.O. Ania, *Chapter 4 Surface chemistry of activated carbons and its characterization*, in *Interface Science and Technology*, J.B. Teresa, Editor. 2006, Elsevier. p. 159-229.
50. Sing, K.S.W., F. Rouquerol, and J. Rouquerol, *5 - Classical Interpretation of Physisorption Isotherms at the Gas–Solid Interface*, in *Adsorption by Powders and Porous Solids (Second Edition)*, F.R.R.S.W.S.L. Maurin, Editor. 2014, Academic Press: Oxford. p. 159-189.
51. McCarty, R.D. and V.D. Arp, *New wide range equation of state for helium*. Advances in Cryogenic Engineering. Vol. 35. 1990. 1465-1475.
52. Hahn, R., et al., *Shallow Bed Adsorption: Theoretical Background and Applications*. Chemical Engineering & Technology, 2005. **28**(11): p. 1241-1251.
53. Lemmon, E.W., McLinden, M.O. and Friend, D.G. . *Thermophysical Properties of Fluid Systems*. NIST Standard Reference Database Number 69; Linstrom, P.J. and Mallard, W.G. :[Available from: <http://webbook.nist.gov>].

54. Brandani, S. and D.M. Ruthven, *Analysis of Zlc Desorption Curves for Liquid-Systems*. Chemical Engineering Science, 1995. **50**(13): p. 2055-2059.
55. Crank, J., *The Mathematics of Diffusion*. 1979: Clarendon Press.
56. Cavalcante, C.L., S. Brandani, and D.M. Ruthven, *Evaluation of the main diffusion path in zeolites from ZLC desorption curves*. Zeolites, 1997. **18**(4): p. 282-285.
57. Rouquerol, F., et al., *1 - Introduction*, in *Adsorption by Powders and Porous Solids (Second Edition)*, F.R.R.S.W.S.L. Maurin, Editor. 2014, Academic Press: Oxford. p. 1-24.
58. Sing, K.S.W., et al., *8 - Assessment of Mesoporosity*, in *Adsorption by Powders and Porous Solids (Second Edition)*, F.R.R.S.W.S.L. Maurin, Editor. 2014, Academic Press: Oxford. p. 269-302.
59. Silvino, P., et al., *Strategies to Improve Pore-size Distribution Characterization of Activated Carbons using CO<sub>2</sub> and N<sub>2</sub> Isotherms: Volume Regularization and Etched Slit Models*. Adsorption Science & Technology, 2013. **31**(2-3): p. 263-274.
60. Davies, G.M., N.A. Seaton, and V.S. Vassiliadis, *Calculation of Pore Size Distributions of Activated Carbons from Adsorption Isotherms*. Langmuir, 1999. **15**(23): p. 8235-8245.
61. Lucena, S.M.P., et al., *The effect of heterogeneity in the randomly etched graphite model for carbon pore size characterization*. Carbon, 2010. **48**(9): p. 2554-2565.
62. Fogler, H.S., *Elements of chemical reaction engineering*. 1999.
63. Ruthven, D.M., S. Brandani, and M. Eic, *Measurement of Diffusion in Microporous Solids by Macroscopic Methods*, in *Adsorption and Diffusion*, H. Karge and J. Weitkamp, Editors. 2008, Springer Berlin Heidelberg. p. 45-84.
64. Silva, J.A.C., F.A. Da Silva, and A.E. Rodrigues, *An Analytical Solution for the Analysis of Zero-Length-Column Experiments with Heat Effects*. Industrial & Engineering Chemistry Research, 2001. **40**(16): p. 3697-3702.
65. Díaz, E., et al., *Adsorption characterisation of different volatile organic compounds over alumina, zeolites and activated carbon using inverse gas chromatography*. Journal of chromatography A, 2004. **1049**(1): p. 139-146.
66. Vargaftik, N.B. and L.V. Yakush, *Temperature dependence of thermal conductivity of helium*. Journal of engineering physics, 1977. **32**(5): p. 530-532.
67. Ruthven, D.M. and S. Brandani, *Measurement of Diffusion in Porous Solids by Zero Length Column (ZLC) Methods*, in *Membrane Science and Technology*, N.K. Kanellopoulos, Editor. 2000, Elsevier. p. 187-212.
68. Huang, Q., et al., *Characterization of the diffusion path in micro- and mesoporous materials from ZLC analysis*. Adsorption, 2010. **16**(6): p. 531-539.